

# Single-Cell Transcriptome Atlas of Murine Endothelial Cells

## Highlights

- A single-cell EC atlas of healthy murine tissues
- This study provides an interactive webtool for comparative analyses and data exploration
- Characterization of inter- and intra-tissue EC heterogeneity
- Discovery tool for characterization of ECs in other datasets

## Authors

Joanna Kalucka, Laura P.M.H. de Rooij, Jermaine Goveia, ..., Xuri Li, Yonglun Luo, Peter Carmeliet

## Correspondence

alun@biomed.au.dk (Y.L.),  
lixr6@mail.sysu.edu.cn (X.L.),  
peter.carmeliet@kuleuven.vib.be (P.C.)

## In Brief

A comprehensive murine atlas comprising >32,000 single endothelial-cell transcriptomes from 11 mouse tissues is reported, and among the subclusters various classical as well as tissue-specialized endothelial-cell subtypes are defined.



# Single-Cell Transcriptome Atlas of Murine Endothelial Cells

Joanna Kalucka,<sup>1,8,10</sup> Laura P.M.H. de Rooij,<sup>1,8</sup> Jermaine Goveia,<sup>1,8</sup> Katerina Rohlenova,<sup>1</sup> Sébastien J. Dumas,<sup>1</sup> Elda Meta,<sup>1</sup> Nadine V. Conchinha,<sup>1</sup> Federico Taverna,<sup>1</sup> Laure-Anne Teuwen,<sup>1</sup> Koen Veys,<sup>1</sup> Melissa García-Caballero,<sup>1</sup> Shawez Khan,<sup>1</sup> Vincent Geldhof,<sup>1</sup> Liliana Sokol,<sup>1</sup> Rongyuan Chen,<sup>2</sup> Lucas Treps,<sup>1</sup> Mila Borri,<sup>1</sup> Pauline de Zeeuw,<sup>1</sup> Charlotte Dubois,<sup>1</sup> Tobias K. Karakach,<sup>1,11,12</sup> Kim D. Falkenberg,<sup>1</sup> Magdalena Parys,<sup>1</sup> Xiangke Yin,<sup>2</sup> Stefan Vinckier,<sup>1</sup> Yuxiang Du,<sup>2</sup> Robert A. Fenton,<sup>3</sup> Luc Schoonjans,<sup>1,2</sup> Mieke Dewerchin,<sup>1</sup> Guy Eelen,<sup>1</sup> Bernard Thienpont,<sup>4</sup> Lin Lin,<sup>3,5</sup> Lars Bolund,<sup>3,5</sup> Xuri Li,<sup>2,9,\*</sup> Yonglun Luo,<sup>3,5,6,7,9,\*</sup> and Peter Carmeliet<sup>1,2,9,13,\*</sup>

<sup>1</sup>Laboratory of Angiogenesis and Vascular Metabolism, Center for Cancer Biology, and Department of Oncology and Leuven Cancer Institute (LKI), VIB and KU Leuven, 3000 Leuven, Belgium

<sup>2</sup>State Key Laboratory of Ophthalmology, Zhongshan Ophthalmic Center, Sun Yat-Sen University, Guangzhou 510060, Guangdong, P.R. China

<sup>3</sup>Department of Biomedicine, Aarhus University, Aarhus 8000, Denmark

<sup>4</sup>Laboratory for Functional Epigenetics, Department of Human Genetics, KU Leuven, 3000 Leuven, Belgium

<sup>5</sup>Lars Bolund Institute of Regenerative Medicine, BGI-Qingdao, Qingdao, Shandong 266555, P.R. China

<sup>6</sup>BGI-Shenzhen, Shenzhen, Guangdong 518083, P.R. China

<sup>7</sup>China National GeneBank, BGI-Shenzhen, Shenzhen, Guangdong 518120, P.R. China

<sup>8</sup>These authors contributed equally

<sup>9</sup>Senior authors; these authors contributed equally

<sup>10</sup>Present address: Aarhus Institute of Advanced Studies (AIAS) and Department of Biomedicine, Aarhus University, Aarhus 8000, Denmark

<sup>11</sup>Present address: Bioinformatics Core Laboratory, Children's Hospital Research Institute of Manitoba, Winnipeg, MB R3E 3P4, Canada

<sup>12</sup>Present address: Rady Faculty of Health Sciences, Department of Pediatrics and Child Health, University of Manitoba, Winnipeg, MB R3T 2N2, Canada

<sup>13</sup>Lead Contact

\*Correspondence: lixr6@mail.sysu.edu.cn (X.L.), alun@biomed.au.dk (Y.L.), peter.carmeliet@kuleuven.vib.be (P.C.)

<https://doi.org/10.1016/j.cell.2020.01.015>

## SUMMARY

The heterogeneity of endothelial cells (ECs) across tissues remains incompletely inventoried. We constructed an atlas of >32,000 single-EC transcriptomes from 11 mouse tissues and identified 78 EC subclusters, including *Aqp7<sup>+</sup>* intestinal capillaries and angiogenic ECs in healthy tissues. ECs from brain/testis, liver/spleen, small intestine/colon, and skeletal muscle/heart pairwise expressed partially overlapping marker genes. Arterial, venous, and lymphatic ECs shared more markers in more tissues than did heterogeneous capillary ECs. ECs from different vascular beds (arteries, capillaries, veins, lymphatics) exhibited transcriptome similarity across tissues, but the tissue (rather than the vessel) type contributed to the EC heterogeneity. Metabolic transcriptome analysis revealed a similar tissue-grouping phenomenon of ECs and heterogeneous metabolic gene signatures in ECs between tissues and between vascular beds within a single tissue in a tissue-type-dependent pattern. The EC atlas taxonomy enabled identification of EC subclusters in public scRNA-seq datasets and provides a powerful discovery tool and resource value.

## INTRODUCTION

Endothelial cells (ECs) line blood vessels and are vital conduits for oxygen and nutrient delivery, immune-cell trafficking, and waste removal to and from distant tissues. The vascular system consists of blood vessels with distinct vascular beds (arteries, capillaries, veins) critical for supplying and draining blood and lymphatic vessels involved in drainage of extravasated fluid (Potente and Mäkinen, 2017). According to a retinal vessel sprouting model, a tip EC navigates the sprout at the forefront, while proliferating stalk ECs elongate the sprout, illustrating an additional level of EC heterogeneity (Potente and Mäkinen, 2017). Further, ECs in different tissues have heterogeneous phenotypes, presumably to meet the distinct physiological needs of each tissue (Augustin and Koh, 2017). For instance, the blood-brain and blood-retinal barrier consist of tightly linked ECs to restrict paracellular diffusion (Sweeney et al., 2018), whereas permeable fenestrations in liver ECs facilitate exchange of solutes (Shetty et al., 2018). Bulk RNA-sequencing (RNA-seq) revealed EC heterogeneity among tissues (Nolan et al., 2013). However, whether and to which extent ECs within a single tissue are phenotypically different at the single cell level and whether, for instance, ECs in a particular vascular bed are heterogeneous across different tissues remains largely unknown.

Some single-cell RNA sequencing (scRNA-seq) studies characterized EC heterogeneity in single tissues (Baryawno et al., 2019; Lukowski et al., 2019; Park et al., 2018; Sabbagh et al.,



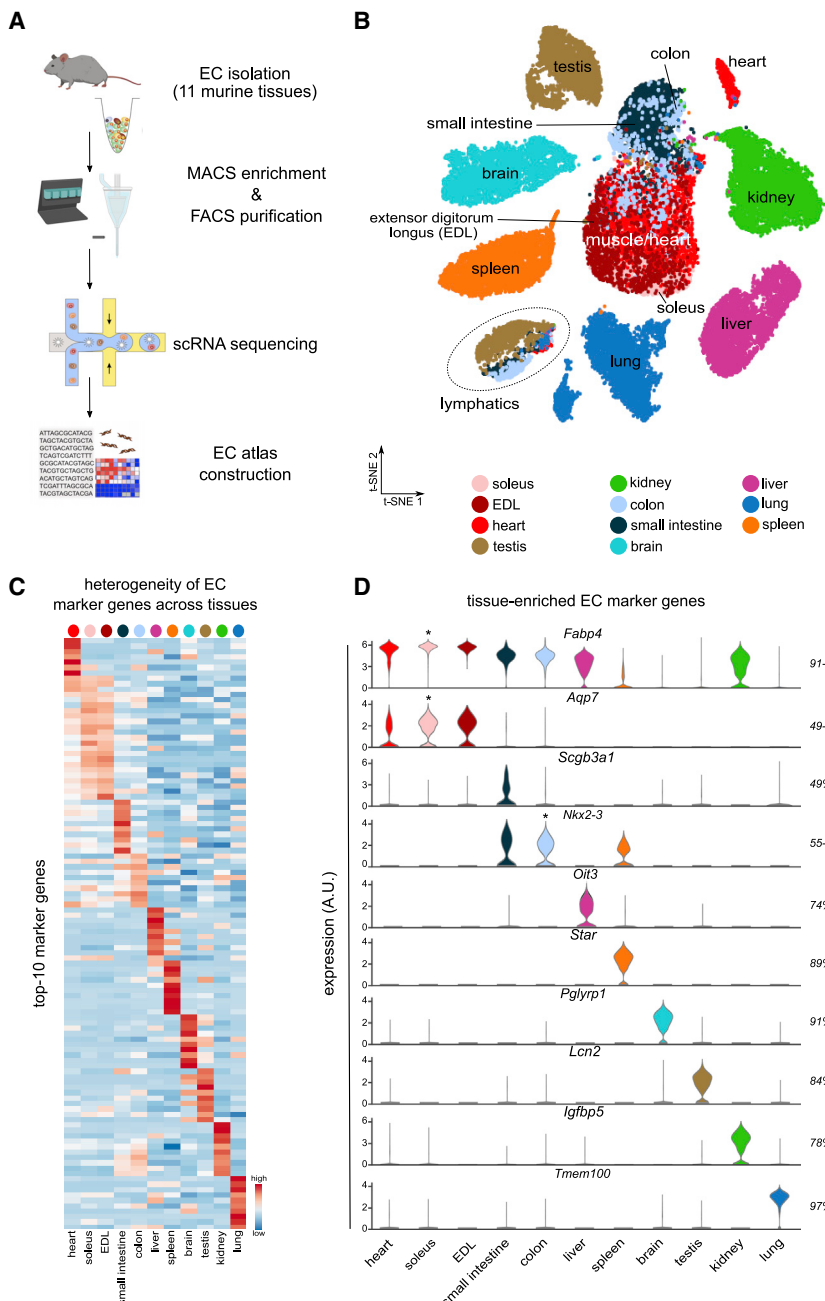


**Figure 1. Tissue-Specific Heterogeneity of ECs**

(A) Scheme of study design.

(B) t-SNE plot of *in silico*-selected ECs, color coded for tissue type.

(C) Gene-expression heatmap of the top 10 marker genes for each tissue. Color scale: red, high expression; blue, low expression.

(D) Violin plots of the expression of markers, highly expressed in a substantial fraction (49% to 100%) of ECs in the indicated tissues (% indicated on the right; in case of marker gene enrichment in multiple tissues, the violin plot with the highest expression is indicated by an asterisk).

Tissues in (C) and (D) are color coded according to t-SNE in (B). A.U., arbitrary units. See Figure S1 and Tables S1 and S2.

## RESULTS

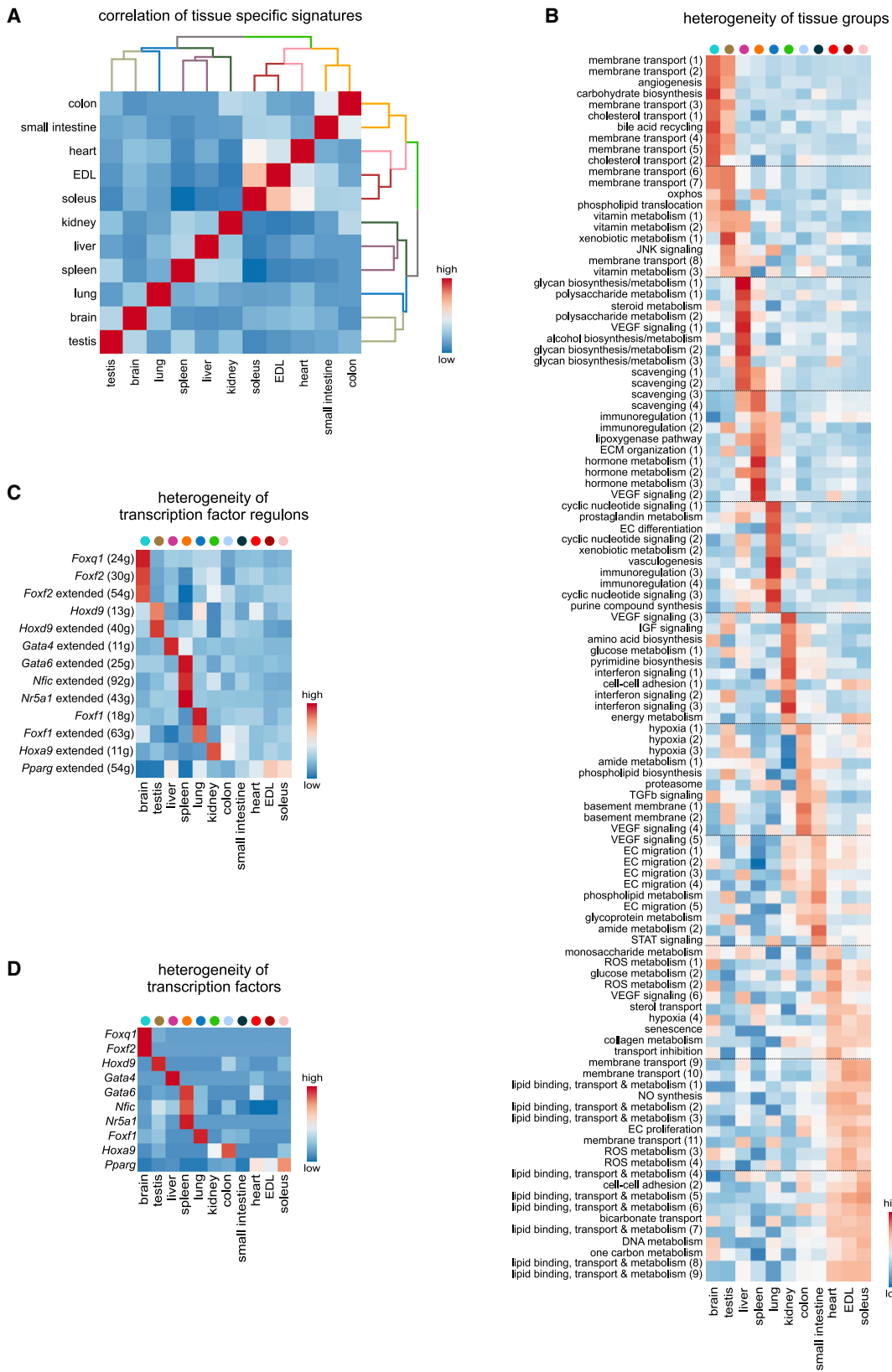
### Construction of the EC Atlas

To efficiently isolate ECs from multiple mouse tissues, we optimized EC isolation and purification protocols (Figure 1A). ECs from each tissue were subjected to scRNA-seq by a 10x Genomics-based single-tube protocol with exclusive transcript counting through barcoding with unique molecular identifiers. We sequenced 39,182 cells and achieved, on average, a sequencing depth of 86,766 reads per cell, sequencing saturation rate of 93%, and 1,308 genes per cell (Table S1).

After quality filtering for the number of detected genes and mitochondrial read counts, duplicates were assessed, and unique transcripts were normalized for total read depth. Subsequently, graph-based clustering was performed to group cells according to their gene-expression profile and t-distributed stochastic neighbor embedding (t-SNE) plots were used for visualization. Next, we selected EC clusters on the basis of the expression of EC markers (*Pecam1*, *Cdh5*) and excluded contaminating smooth muscle cells (*Acta2*), fibroblasts (*Col1a1*), and red blood

cells (*Hba-a1*, *Hba-a2*, *Hbb-bs*) (Figures S1A and S1B). Cells expressing markers of pericytes (*Pdgfrb*) or immune cells (*Ptprc*) were absent. We obtained a total of 32,567 ECs from 11 tissues (83% of all cells sequenced) (Figure S1C).

ECs from different tissues exhibited prominent transcriptomic heterogeneity (Figure 1B). Lymphatic ECs (LECs) are functionally and anatomically distinct from blood vascular ECs (referred to as “BECs” or “ECs”). Because the primary goal of this study was to focus on BECs, and because we obtained more BECs than LECs (Figure S1A), we only briefly characterized LECs and identified differentially expressed marker genes (Figure S1D; Table S2).



(legend on next page)

We then used a rank product-based method to identify enriched EC marker genes for each tissue (Breitling et al., 2004) (Table S2). Heatmap analysis of the top-10-ranking markers revealed distinct signatures of ECs from each tissue, except for the soleus and extensor digitorum longus (EDL) skeletal muscles, which expressed overlapping marker genes (Figure 1C; Table S2). Of note, some of these top marker genes were expressed by ECs from only a single tissue (*Pglyrp1*, *Lcn2*, and *Tmem100* in brain, testis, and lung, respectively), whereas other EC markers (*Fabp4*, *Aqp7*, *Nkx2-3*) were conserved across two or more tissues (Figure 1D). Most of these markers were expressed by a substantial fraction of ECs from a particular tissue (Figure 1D). The expression of common markers by ECs from more than one tissue raised the question as to whether these ECs were phenotypically related to each other (see below).

### Inter-tissue Heterogeneity of Blood Vascular ECs

To study EC heterogeneity across tissues, we first used hierarchical clustering complemented with multiscale bootstrap resampling. This analysis revealed that ECs from certain tissues (testis and brain; liver and spleen; small intestine and colon; skeletal muscle soleus and EDL) clustered together on the dendrogram, suggesting partially overlapping transcriptome signatures (Figure 2A).

In an attempt to explain this phenomenon of tissue grouping of ECs, we performed gene set variation analysis (GSVA) with an in-house generated list of 615 vascular related gene sets that were selected from the Molecular Signatures Database (MSigDB) (Table S3). Heatmap analysis of the top-10-ranking expressed gene sets (Figure 2B; Table S3) revealed that ECs from these tissues highly expressed gene sets involved in different biological processes (for complete list of gene sets and GSVA scores, see Table S3). Indeed, brain and testis ECs highly expressed gene sets involved in transmembrane transport, in agreement with the existence of a blood-tissue barrier (Su et al., 2011; Sweeney et al., 2019). Liver and spleen ECs highly expressed gene sets involved in scavenging and immunoregulation, in line with previous reports (Blum et al., 2013; Bronte and Pittet, 2013; Fraser et al., 1997). Colon and small intestine ECs highly expressed gene sets involved in vascular basement membrane/collagen deposition, VEGF signaling, and EC migration (gene sets that are also involved in vascular barrier integrity and maintenance [Lee et al., 2007; Murakami et al., 2008]), in agreement with their known role in the maintenance of the gut vascular barrier (Spadoni et al., 2015). The cardiac EC transcriptome largely resembled that of skeletal muscle ECs. Gene sets involved in membrane transport and redox homeostasis were enriched, in line with the highly oxidative microenvironment of

the heart (Doenst et al., 2013). Lung ECs showed an enrichment of immunoregulatory-related signatures, suggesting a putative role in immune surveillance. Kidney ECs expressed gene sets involved in signaling activated by interferon. Intriguingly, most ECs from these tissues expressed distinct metabolic gene signatures (see below for further analysis).

### Transcription Factor Network Analysis

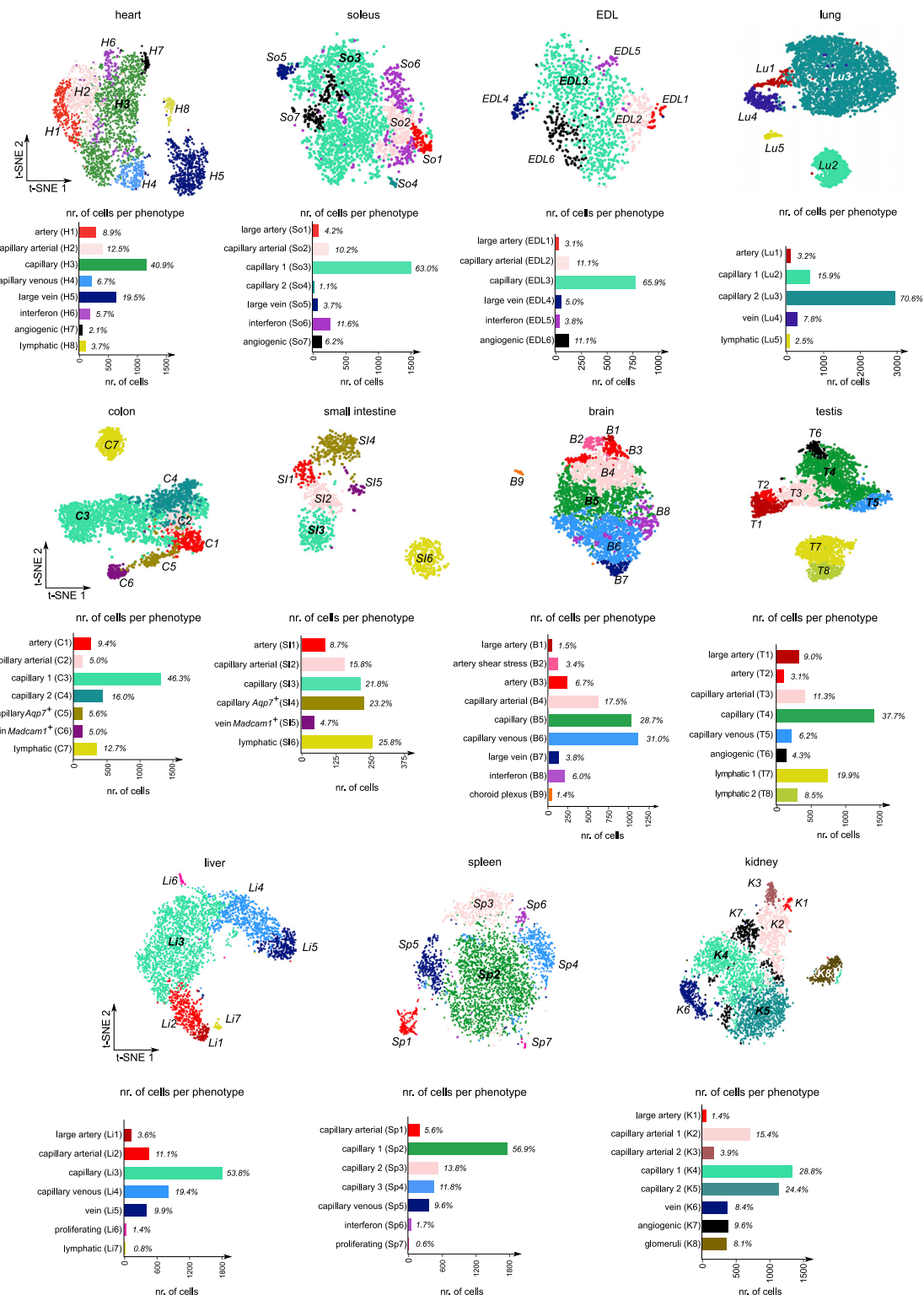
To study the underlying molecular mechanisms driving the differentiation of the different EC phenotypes, we used single-cell regulatory network inference and clustering (SCENIC) (Aibar et al., 2017). This analysis predicted that ECs from different tissues upregulated the expression of different transcription-factor networks. For instance, *Foxq1* and *Hoxd9* regulons were upregulated in ECs from brain and testis, respectively, whereas a *Foxf1* network was enriched in pulmonary ECs, and skeletal muscle ECs showed increased activity of a *Pparg* network (Figure 2C). Regulons driven by transcription factors of members of the Gata family were enriched in ECs from liver and spleen. In line with reports that *Gata4* and *Gata6* are essential for liver development (Watt et al., 2007), and *Gata4* expression in adult mouse liver is restricted to ECs (Divine et al., 2004), a *Gata4* network was upregulated in liver ECs, whereas a *Gata6* regulon was predominantly detected in splenic ECs (Figure 2C). Splenic, but not liver ECs, also upregulated networks driven by *Nr5a1* and *Nfic* (Figure 2C). Heatmap-expression analysis confirmed transcript upregulation of these transcription factors (Figure 2D).

### Vascular-Bed Heterogeneity within Tissues

We studied intra-tissue EC heterogeneity by graph-based subclustering of ECs for each tissue separately. We show the expression of the top 20 (Figures S2–S4) or top 50 (Table S2) marker genes for each tissue-specific EC subcluster, the number of unique molecular identifiers (UMIs) and genes per tissue (Figures S2–S4), and the relative fraction of each EC subcluster (Figure 3). Each tissue-specific EC subcluster was given a specific annotation (H1 for heart subcluster 1, etc.) (Table S2). Comparable results were obtained when using t-SNE (Figure 3) or uniform manifold approximation and projection (UMAP) (Figure S5A) for visualization. For annotation of the EC subclusters and to infer a putative function, we analyzed the differential expression of established (canonical) markers of different EC subtypes. For instance, in some arterial and venous EC clusters, we identified enrichment of large vessel markers (*Vwf*, *Vcam1*), the expression level of which correlates with the vessel diameter (Gustavsson et al., 2010)—we therefore putatively classified them as “large artery/vein” ECs (see also pseudotime analysis below). Also, reports show that arteriolar ECs express both arterial and capillary

### Figure 2. Inter-tissue Heterogeneity of ECs

- (A) Correlation heatmap and hierarchical clustering of EC gene-expression signatures of all tissues. Color differences in the dendrogram indicate clusters that were resolved by multiscale bootstrapping.
  - (B) Heatmap showing processes enriched in different tissues. Gene-set signatures involved in similar processes were given a common name, followed by a number (between brackets) according to their order of appearance in the heatmap. Color coding from t-SNE in Figure 1B is shown above the heatmap.
  - (C) Heatmap of the inferred transcription-factor gene-regulatory networks (SCENIC). Numbers between brackets indicate the (extended) regulons for respective transcription factors.
  - (D) Gene-expression heatmap of transcription factors in (C). Color scale: red, high expression; blue, low expression.
- See also Table S3.

**Figure 3. Vascular-Bed Heterogeneity across Tissues**

t-SNE plot visualization of tissue-specific EC subclusters, color coded for the identified EC phenotypes. Each cluster was numbered and labeled with the first letter(s) of the tissue name (H1 for subcluster 1 in heart, etc.). Annotations of the top-ranking marker genes of each cluster are provided in Figures S2–S4. Bar graphs showing the number of cells and the relative fraction (%) of each EC subcluster in the tissue-specific ECs are provided below the t-SNE plots. See also Figures S2–S5 and Table S2.

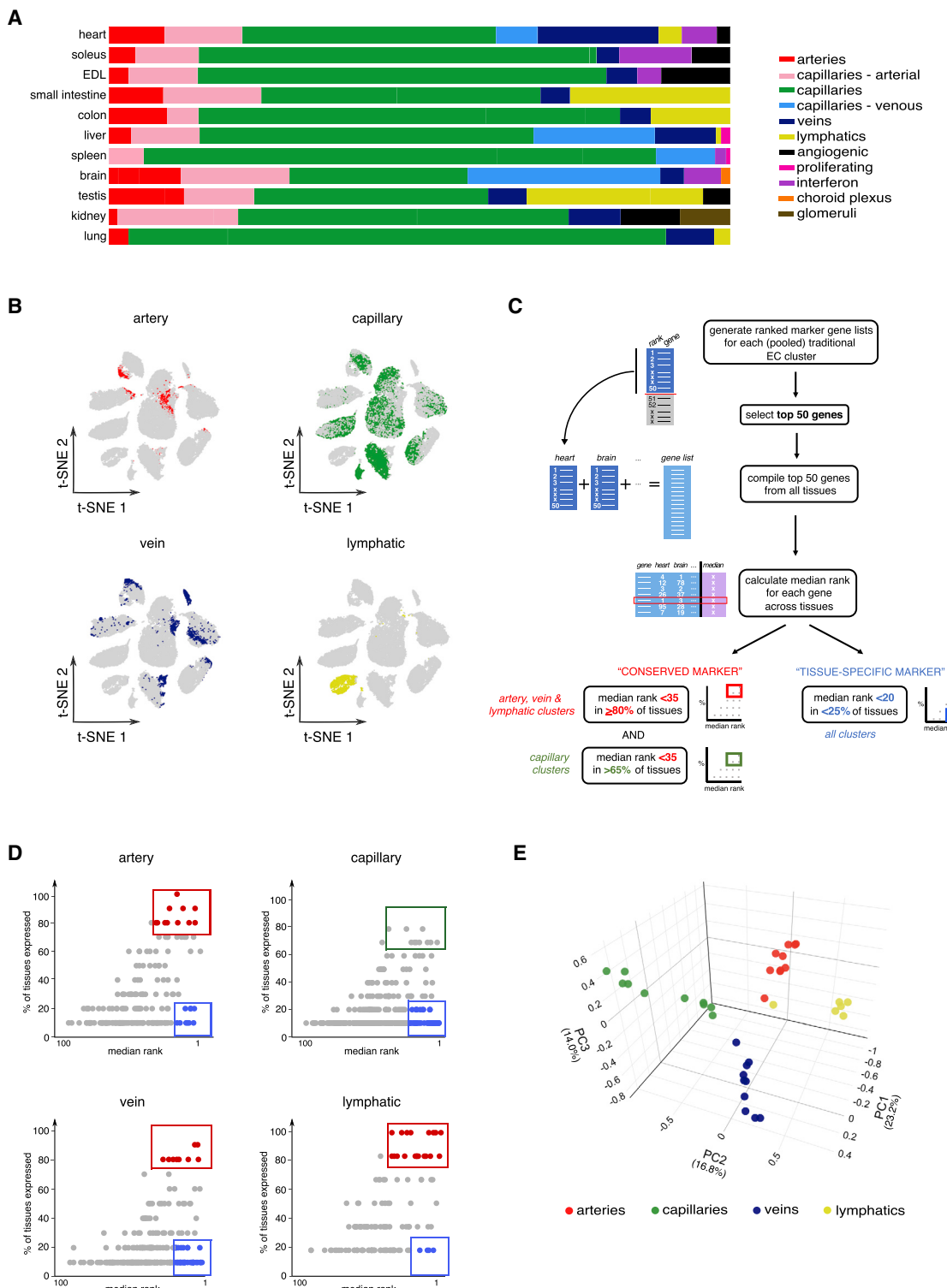


**Figure 4. Conserved and Tissue-Specific Marker Genes of EC Subtypes**

(A) Relative fraction of EC subclusters in different tissues. The relative contribution of each population was weighed by the number of cells per tissue and scaled to 100%.

(B) t-SNE plots, color coded for EC subclusters from traditional vascular beds, across tissues.

(C) Scheme of conserved and tissue-specific marker identification.

(legend continued on next page)

markers (Pusztaszeri et al., 2006; Zhao et al., 2018), consistent with their topographical location along the vascular tree (in between arteries and capillaries). We therefore named arteriolar ECs “capillary-arterial” ECs. Similarly, because venular ECs express venous and capillary markers (Pusztaszeri et al., 2006; Zhao et al., 2018), we coined venular ECs “capillary-venous” ECs.

To obtain independent evidence for the putative topography of the various EC subclusters alongside the vascular tree, we performed pseudotime analysis to predict the differentiation trajectory of these EC subclusters. This analysis predicted a trajectory from arteries, over capillaries, to veins (Figure S5B). To map the location of (other) EC subclusters on the pseudotime trajectory, we focused on brain ECs, because we used markers of arterial, capillary, and venous ECs, identified in a reference scRNA-seq dataset of brain ECs (Vanlandewijck et al., 2018) or established in previous studies (Fischer et al., 2004; Ghadour et al., 1992; Gustavsson et al., 2010) (Figures S5C and S5D). Expression of known brain arterial EC marker genes (*Gkn3*, *Hey1* [Fischer et al., 2004; Vanlandewijck et al., 2018]) was detected at the arterial end of the pseudotime trajectory, whereas expression of the known brain vein marker *Slc38a5* (Vanlandewijck et al., 2018) was enriched at the venous end of the trajectory (Figure S5D). At the far ends of the pseudotime trajectory, expression of the large vessel markers *Vwf* and *Vcam1* (Gustavsson et al., 2010) was highest in ECs from arteries and veins; these ECs therefore likely represent large arteries and veins (Figure S5C). The capillary marker gene *Mfsd2a* (Vanlandewijck et al., 2018) was enriched most in the middle part of the pseudotime trajectory, whereas the capillary-arterial marker *Tgfb2* and capillary-venous marker *Tfrc* (Vanlandewijck et al., 2018) were identified at the capillary-arterial and capillary-venous transition points along the trajectory, respectively (Figure S5D). This analysis also revealed *Fbln5* and *Cyt1* as large artery markers, *Glul* as a capillary-arterial marker, *Rgcc* as a capillary marker, *Car4* as a capillary-venous marker, and *Lcn2* as a large vein marker in the brain (Figure S5D). Hence, *in silico* lineage tracing using single-cell transcriptomes captured the anatomical topography of the various EC subtypes in distinct vascular beds.

In total, we identified 78 distinct EC populations across all tissues (Figure 3; Figure S5A), including (1) traditional EC phenotypes (artery, capillary, vein, and lymphatic ECs), detected at variable numbers in different tissues; (2) tissue-restricted EC populations (choroid plexus in brain; *Madcam1*<sup>+</sup> veins and *Aqp7*<sup>+</sup> capillaries in intestines); and (3) unexpected EC phenotypes, such as interferon-activated ECs in brain, spleen, muscle, and heart; angiogenic ECs in heart, muscle, testis, and kidney; and proliferating ECs in liver and spleen.

We evaluated differences/similarities between ECs in distinct vascular beds (arteries, capillaries, veins, lymphatics), which comprised the largest fraction of ECs, across different tissues (Figures 4A and 4B). To capture the EC heterogeneity, we used complementary approaches. First, we explored which EC

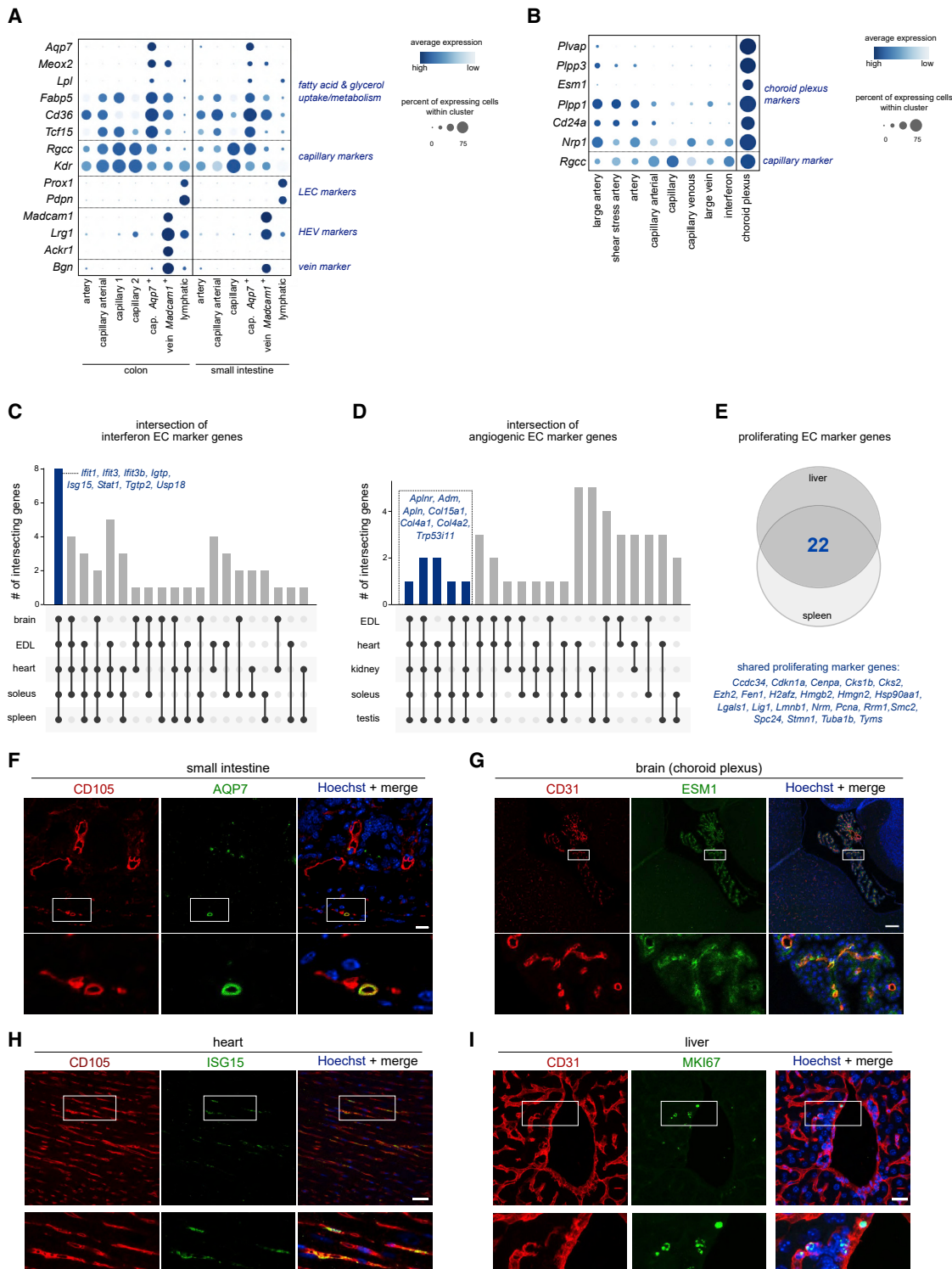
markers in these vascular beds were conserved between tissues or expressed in a tissue-specific manner. For each tissue, we therefore pooled clusters into the following EC phenotypes: (1) arterial ECs (containing large artery and artery EC subclusters), (2) capillary ECs (all capillary EC subclusters), (3) venous ECs (large vein and vein EC subclusters), and (4) lymphatic ECs (all lymphatic EC subclusters) (Figure 4B; Table S4). ECs expressing genes of two vascular beds (capillary-arterial and capillary-venous ECs), as well as ECs restricted to only some tissues, were not included (see STAR Methods). We then calculated the median rank score of the top-50-ranked markers in every pooled EC subcluster across tissues. Marker genes with a median rank of <35 that were identified in ≥80% of all tissues were considered conserved vascular bed markers (Figures 4C and 4D; Table S5). We identified multiple conserved markers for arteries, veins, and lymphatics but detected fewer conserved markers for capillaries, highlighting a greater heterogeneity of capillary EC markers across tissues (Figures 4C and 4D). When analyzing tissue-specific vascular bed markers with a median rank <20 identified in <25% of all tissues (corresponding to one or two tissues) (Figures 4C and 4D), we identified more tissue-specific markers for capillaries than for lymphatics (Figures 4C and 4D). This raises the question as to whether capillary ECs adapt more flexibly to the tissue microenvironment to meet tissue-specific needs, in contrast to the more general role of lymphatics to drain extravasated fluid, regardless of their tissue microenvironment.

Second, to explore whether ECs from the same vascular bed (arteries, capillaries, veins, lymphatics) across different tissues resembled each other transcriptomically, we used the Jaccard similarity analysis to score the similarity of the top-50-ranking marker gene sets of the pooled arterial, capillary, venous, and lymphatic ECs from different tissues (Figure 4E; Table S4). This analysis showed that the transcriptome signature of arterial ECs was relatively similar across tissues and differed from the transcriptome signature of capillary, vein, or lymphatic ECs. Similar findings were obtained for capillary, vein, and lymphatic ECs (Figure 4E). Rephrased, transcriptomically, ECs from a particular vascular bed are relatively similar across tissues and more similar to each other than to ECs from other vascular beds.

This analysis does, however, not address the question as to whether the tissue-specific EC heterogeneity is determined by the tissue of origin or the vessel subtype. We therefore performed hierarchical clustering of all EC subclusters across tissues. As evident from the dendrogram, EC subclusters were grouped per tissue, not per vessel type, suggesting that the tissue type (rather than the vessel type) contributes to the EC heterogeneity (Figure S5E).

Lastly, we assessed the expression pattern of conserved and tissue-specific EC marker genes in non-endothelial cell types, taking advantage of the publicly available *Tabula Muris* datasets from heart, brain, limb muscle, liver, kidney, and lung (Tabula Muris Consortium et al., 2018). For each tissue, we could detect

(D) Dot plots of conserved and tissue-specific markers in ECs from the distinct vascular beds in different tissues. Red boxes, conserved markers between ECs from different tissues; blue boxes, tissue-specific markers; green box, capillary markers conserved across >65% of tissues. Dots: individual marker genes.  
 (E) Three-dimensional PCA visualization of pairwise Jaccard similarity coefficients between ECs from distinct vascular beds in different tissues. See Figures S5 and S6; Tables S4 and S5.

**Figure 5. Specialized and Unexpected EC Phenotypes**

(A and B) Dot-plot heatmap of markers enriched in intestinal *Aqp7*<sup>+</sup> capillary and *Madcam1*<sup>+</sup> vein ECs (A) and brain *Plvap*<sup>+</sup>/*Esm1*<sup>+</sup> choroid plexus capillary ECs (B); these EC subclusters were named after their most specifically expressed marker(s) (respectively *Aqp7*, *Madcam*, and *Plvap/Esm1*). The color intensity of each dot represents the average level of marker expression, whereas the dot size reflects the percentage of ECs expressing the marker within the EC subcluster.

(legend continued on next page)

genes that were expressed at a higher level ( $>0.5 \log_2$ -fold change) in ECs than in other cell types (Figure S6).

### Intra-tissue Profiling Reveals Specialized EC Phenotypes

We then focused on ECs with specialized biological features, detected in only a subset of tissues and a fraction of ECs in these tissues. Based on marker gene expression (Figures S2–S4), all specialized EC phenotypes, except one venous EC phenotype, expressed capillary markers, further illustrating the plasticity of capillary ECs. Table S2 lists the top 50 marker genes of these specialized EC phenotypes.

In intestines, we identified a fraction (5.6%–23.2%) of capillary ECs with elevated transcript levels of genes involved in the uptake and metabolism of glycerol and fatty acids (*Aqp7*, *Tcf15*, *Cd36*, *Fabp5*) (Figures 3 and 5A). Although at first sight transcriptomically resembling lacteal ECs (lymphatic vessels specialized in transport of dietary fat from intestines to blood [Dixon, 2010]), these ECs did not express traditional lymphatic markers (*Prox1*, *Pdpn*) (Figure 5A). We therefore refer to this subcluster as *Aqp7<sup>+</sup>* capillary ECs (subcluster C5 and SI4 in Figure 3; Figure S5A). Capillary ECs in other tissues (heart, skeletal muscle) ubiquitously express AQP7 (Skowronski et al., 2007), but expression of AQP7 in intestinal capillary ECs has not been reported yet, likely because it is only expressed in a fraction of these cells. Nonetheless, *Aqp7<sup>+</sup>* capillary ECs might have a particular physiological role (see Discussion). In addition, as illustrated in Figure 5A, we identified a fraction (4.7%–5.0%) of intestinal venous ECs (identified by expression of the venous EC marker *Bgn*), which exhibited enriched expression of high-endothelial venule (HEV) markers (*Madcam1*, *Lrg1*, *Ackr1*) (Kashiwazaki et al., 2003; Saito et al., 2002) (C6 and SI5 in Figure 3; Figure S5A), representing a specialized subtype of ECs adapted for recruiting/trafficking of lymphocytes from blood to the tissue interstitium (Girard et al., 2012).

In brain, we identified a small (1.4%) subcluster of choroid plexus capillary ECs (B9 in Figures 3 and 5A), characterized by elevated expression of the known marker gene *Plvap* (Figure 5B), in agreement with reports describing fenestrated capillaries involved in the production of the cerebrospinal fluid (Bosma et al., 2018). Apart from other markers (*Plpp1*, *Plpp3*, *Cd24a*, *Nrp1*), we also detected enriched expression of *Esm1* (Figure 5B), a known marker of choroid plexus capillary ECs at the mRNA level (Bowyer et al., 2013) but not yet validated at the protein level.

We also detected ECs that we had not expected in the quiescent endothelium of healthy organs. For instance, a population (1.7%–11.6%) of capillary ECs exhibiting an interferon response,

termed “interferon-activated ECs” (B8, EDL5, H6, and So6, and Sp6 in Figure 3; Figure S5A), was identified in brain, heart, muscle, and spleen. When focusing on the top 50 marker genes expressed by each of these 5 tissues, we detected a subset of 8 common interferon-induced genes, raising the question as to whether in these tissues interferon signaling might play a role in healthy EC homeostasis (Figure 5C, blue bar; Table S6).

Equally unexpectedly, we identified a population (2.1%–11.1%) of capillary ECs expressing an angiogenic gene-expression signature in heart, skeletal muscle, kidney, and testicular ECs (K7, H7, EDL6, and So7, and T6 in Figure 3; Figure S5A). Analysis of their top 50 marker genes revealed a subset of 7 genes commonly upregulated in 4 out of 5 tissues harboring angiogenic ECs (Figure 5D, blue bars; Table S6), some of which have been reported as tip cell-enriched marker genes in tumor vessels (*Apln*, *Co4a2*, *Trp53i11* [Zhao et al., 2018]). Notably, angiogenic ECs in these different tissues did not always express the same markers, further illustrating the EC heterogeneity.

Moreover, in liver and spleen, proliferating capillary ECs, expressing typical proliferation markers (cyclin-dependent kinases, high-mobility group proteins, others), were identified at respectively 1.4% and 0.6% (Li6 and Sp7 in Figure 3; Figure S5A). In total, 22 genes were commonly expressed by these two EC phenotypes (Figure 5E; Table S6).

Double immunostaining for an EC marker (CD105 or CD31) and a marker of these specialized EC phenotypes confirmed the scRNA-seq data (Figures 5F–5I; Figures S7A–S7G).

### Inter-tissue EC Heterogeneity of Metabolic Gene Signatures

Because an unbiased approach revealed that distinct metabolic genes were upregulated in ECs from different tissues and co-determined the tissue grouping phenomenon of ECs (Figures 2A and 2B), and metabolism of ECs regulates vessel homeostasis and growth (Falkenberg et al., 2019; Li et al., 2019), we further explored the heterogeneity of metabolic gene-expression signatures of ECs in vascular beds across tissues. Focusing on metabolic genes only, hierarchical clustering complemented with multiscale bootstrap resampling revealed similar tissue grouping of ECs (Figure 6A) as obtained when using both non-metabolic and metabolic genes (Figure 2A), suggesting that the metabolic transcriptome signature contributed to the tissue-grouping phenomenon of ECs.

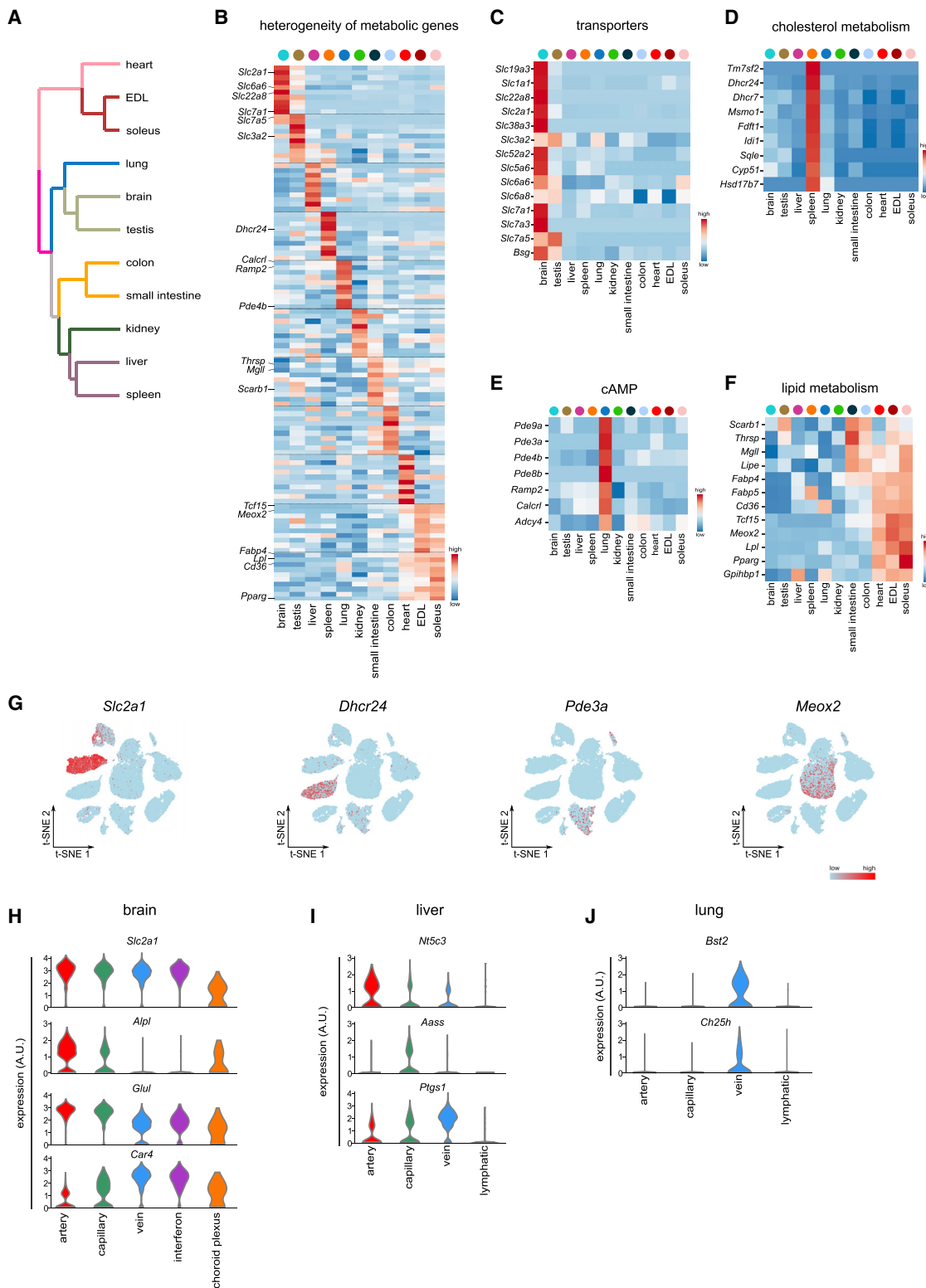
Using all 1,180 detectable metabolic genes in ECs and performing heatmap analysis of the expression levels of the top-10-ranking metabolic-gene transcripts, we observed that ECs from different tissues upregulated the expression of distinct sets of metabolic genes, except for the soleus and EDL skeletal

(C and D) UpSet plot of intersections between the top 50 markers expressed by interferon-activated (C) and angiogenic (D) ECs from the indicated tissues. Blue bar: intersecting genes (listed in blue), commonly detected in all or the majority of the tissues containing respectively the interferon-activated or angiogenic ECs. Black connected dots beneath the graph indicate which tissue clusters are intersected (highly expressing these markers).

(E) Venn diagram showing genes upregulated in proliferating ECs. The number of congruently upregulated genes is indicated in the middle, their gene symbols are listed at the bottom.

(F–I) Representative micrographs of mouse tissue sections, stained for an EC marker (CD105 in F and H; CD31 in G and I) and AQP7 (small intestine, F), ESM1 (choroid plexus, G), ISG15 (heart, H), and MKI67 (liver, I) and counterstained with Hoechst. Lower panels represent magnifications of the respective boxed areas in the upper panels. Scale bars, 10  $\mu\text{m}$  (F); 250  $\mu\text{m}$  (G); 25  $\mu\text{m}$  (H and I).

See also Figure S7 and Tables S2 and S6.

**Figure 6. Inter-tissue EC Heterogeneity of Metabolic Gene Signatures**

(A) Hierarchical clustering analysis of metabolic genes for all tissues. Color differences in the dendrogram indicate clusters that were resolved by multiscale bootstrapping.

(B) Heatmap showing the expression of the top 10 metabolic genes enriched in ECs from different tissues.

(legend continued on next page)

muscle ECs (Figure 6B; Table S7). Focusing on multiple genes within a single metabolic pathway, we observed that ECs from brain (and, to a lesser extent, of testis) upregulated the expression of transporters that were involved in the transport of glucose (*Slc2a1* [Sahoo et al., 2014]), amino acids (*Slc3a2*, *Slc7a5* [Kanai et al., 1998]), and fatty acids (*Bsg* [Muramatsu and Miyauchi, 2003]) (Figures 6C and 6G; Table S7). Splenic ECs upregulated the expression of genes involved in cholesterol metabolism (Sharpe and Brown, 2013) (Figures 6D and 6G; Table S7), in line with reports that the spleen might regulate plasma cholesterol levels (Asai et al., 1988), though these studies did not implicate any contribution of splenic ECs. Further, lung ECs upregulated the expression of genes involved in cAMP metabolism (Bender and Beavo, 2006; Kamitani et al., 1999) (Figures 6E and 6G; Table S7), supporting the notion that the integrity of the pulmonary endothelium depends on cAMP levels (Sayner, 2011). Lastly, cardiac and muscle ECs (and to a lesser extent intestinal ECs) expressed higher transcript levels of genes involved in lipid uptake and metabolism (Bharadwaj et al., 2010; Iso et al., 2013) (Figures 6F and 6G; Table S7), in agreement with reports that triglycerides are taken up by muscle ECs to provide cargo and energy for muscle function (Watt and Hoy, 2012).

We next assessed another level of EC heterogeneity, namely whether ECs from different vascular beds within a single tissue upregulated transcripts of different metabolic marker genes and whether this occurred in a tissue-dependent manner. Rather than providing an all-encompassing overview in all tissues, we highlight this complex heterogeneity by illustrating some typical examples. For instance, in brain, the expression of transporter genes was upregulated in arterial, capillary, vein, and interferon-activated ECs but not in choroid plexus ECs (Figure 6H). The expression of the *Apl* marker was primarily upregulated in arterial ECs, whereas transcript levels of *Glul* were additionally high in capillary ECs, yet another marker (*Car4*) was highly expressed in veins, capillaries, and interferon-activated ECs but less so in arteries (Figure 6H). Vascular-bed ECs in liver differed from all other tissues, because each vascular bed in this tissue upregulated the expression of distinct markers in one vascular bed and only minimally/much less in the other vascular beds (*Nt5c3* in arteries, *Aass* in capillaries, *Ptg51* in veins) (Figure 6I). In lung, veins distinguished themselves from other vascular beds by upregulating the expression of particular metabolic markers (Figure 6J). Thus, ECs show heterogeneity in metabolic gene expression in different vascular beds in a single tissue, in a tissue-dependent pattern.

#### Usefulness of the EC Atlas Taxonomy to Identify EC Phenotypes in Other Datasets

We explored how generally useful the EC Atlas taxonomy is to identify EC phenotypes in other publicly available scRNA-seq

datasets. We used ECs from the *Tabula Muris* liver, heart, brain, kidney, hindlimb muscle, and lung datasets. By using scmap (Kiselev et al., 2018) and the top 10 marker genes of each EC phenotype, nearly all ECs could be confidently assigned to one of the tissue-specific EC phenotypes detected in the EC Atlas taxonomy (Figure 7A). Of note, we did not detect a gender-specific bias toward the presence of different EC phenotypes in the EC Atlas, because *Tabula Muris* ECs from both male and female mice contributed to each EC phenotype of the EC Atlas. Indeed, hierarchical clustering and multiscale bootstrap resampling (using the same top 10 marker genes as described above) of all EC subclusters in tissues from male and female mice confirmed that scmap-annotated EC populations from both genders coincided (Figure 7B). Similar results were obtained when using scmap to assign EC Atlas-identified EC phenotypes to additional publicly available scRNA-seq EC datasets from brain (Vanlandewijck et al., 2018), lung (He et al., 2018), and heart (Zhao et al., 2018) (Figures 7C–7E).

#### DISCUSSION

This study revealed novel insights in various aspects. First, we identified top-ranking marker genes that were highly enriched in a large majority of ECs from brain, testis, and lung (Figure 1D). ECs from other tissues shared at least two or more top-ranking marker genes (Figure 1D). Second, based on findings of partially overlapping transcriptome signatures and shared inferred putative biological features, we propose a new classification of ECs in functionally or anatomically related tissues (brain/testis, liver/spleen, small intestine/colon, and skeletal muscle/heart). Our study thus differs from a previous bulk RNA-seq study of mouse organ ECs, which documented transcriptome similarities of ECs between heart and muscle but not between other tissues (Nolan et al., 2013). We illustrate the concept of tissue grouping of ECs with a few examples. For instance, consistent with their known blood-tissue barrier to secure strict homeostasis of the microenvironment and tight control of trans-endothelial cellular migration and solute transport (Su et al., 2011; Sweeney et al., 2019), brain and testis ECs highly expressed genes involved in transport processes. ECs from liver and spleen upregulated genes involved in scavenging and immuno-regulation, in agreement with their known role in scavenging pathogens, dead cells, and molecules (Qiu et al., 2018; Seternes et al., 2002) and the fact that the spleen regulates immune responses against pathogens (Bronte and Pittet, 2013), and the liver is under constant threat of an invasion by intestinal pathogens into the circulation (Poisson et al., 2017). ECs from especially the lung highly expressed MHC class II genes, suggesting a role in immune surveillance (Goveia et al., 2020). Because ECs represent the first contact for pathogens and immune cells, it is not illogical that they must be equipped with the machinery to mount adequate immune responses

(C–F) Tissue-specific EC expression heatmaps of representative metabolic genes involved in transport (C), cholesterol metabolism (D), cAMP metabolism/biosynthesis (E), and lipid metabolism (F).

(G) t-SNE plots showing upregulated expression of representative metabolic genes (in red) for different tissues.

(H–J) Violin plots showing the expression of representative metabolic marker genes for brain (H), liver (I), and lung (J) EC phenotypes, showing the distribution of expression levels of the selected metabolic marker genes in different vascular beds.

A.U., arbitrary units. Color scales: red, high expression; blue, low expression. See also Table S7.

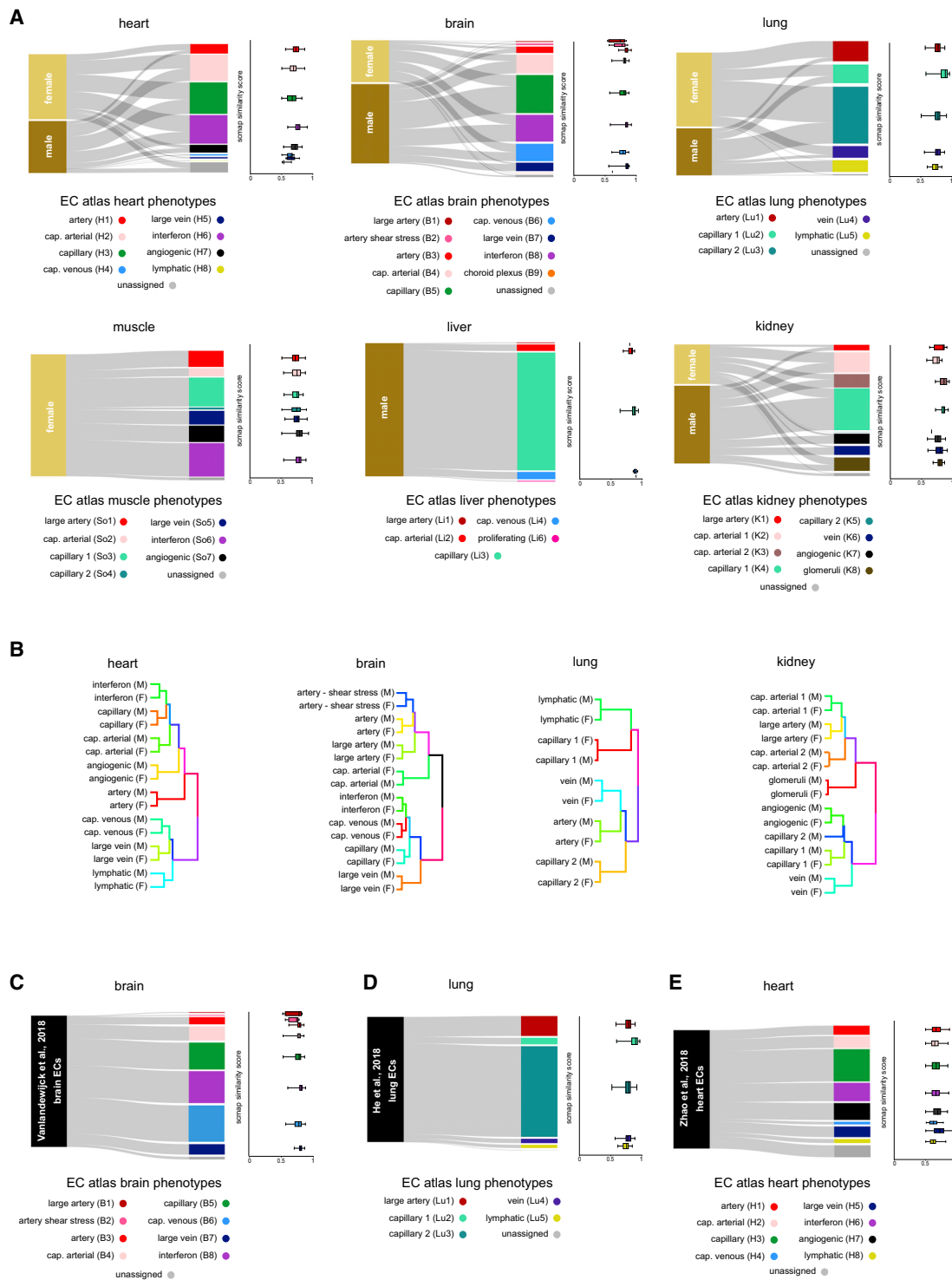


**Figure 7. Annotation of ECs from Publicly Available EC Datasets Using the EC Atlas Taxonomy**

(A) Sankey diagrams, showing the scmap cluster projection of the *Tabula Muris* ECs in different tissues to the EC Atlas taxonomy; *Tabula Muris* ECs are annotated according to mouse gender. Similarity scores of *Tabula Muris* ECs for each EC Atlas EC subcluster per tissue are shown in boxplots. Unassigned cells are indicated in gray. Soleus and EDL ECs from the EC Atlas were pooled and denoted “EC Atlas muscle.”

(legend continued on next page)

(Mai et al., 2013; Wohleber and Knolle, 2016). This is especially relevant for lung and gut, which are exposed to airborne and dietary pathogens. An outstanding question is whether the high expression of genes involved in antigen presentation by lung ECs can explain the more severe graft rejection of transplanted lungs than of other organs (Martinu et al., 2009) and clarify findings that blocking MHC class II on ECs attenuates tissue rejection (Abrahimi et al., 2016). Another finding was that ECs from intestines upregulated the expression of genes involved in vascular integrity, in agreement with their role in the maintenance of the gut vascular barrier that supports nutrient exchange and prohibits access of intestinal microbes to the circulation (Demanan and Rescigno, 2009; Spadoni et al., 2015). Also, kidney ECs expressed gene sets involved in signaling cascades, including signaling activated by interferon, raising the question as to whether they are involved in balancing the expression of genes involved in inflammation, essential for the homeostasis of the renal vascular bed (Jourde-Chiche et al., 2019; Dumas et al., 2020). ECs from each tissue group obviously expressed also non-overlapping gene sets.

Third, across all tissues analyzed, ECs from each vascular bed (artery, capillary, vein, lymphatic) grouped together in a Jaccard similarity analysis, implying that, across tissues, ECs from each vascular bed transcriptomically resembled each other more than ECs from another vascular bed did. Hierarchical clustering of all EC subclusters across tissues revealed, however, that the tissue type of origin (rather than the vessel type) predominantly contributed to the tissue-restricted EC heterogeneity. In search for vascular-bed-specific markers across tissues, we identified markers for arteries, veins, and lymphatics that were shared by 80% to 100% of tissues, indicating phenotypic conservation of these vascular-bed EC markers across tissues. Capillary ECs exhibited more tissue-type-dependent phenotypic variation, raising the question as to whether capillary ECs could thus be more plastic to adapt to the tissue micro-environment in order to meet the different physiological needs of each distinct tissue. This might not be too surprising, because physiologically relevant processes (nutrient and waste exchange, etc.) occur primarily at the capillary level, whereas arteries, veins, and lymphatics are involved more in the supply and drainage of these constituents. Nonetheless, each of these vascular beds also expressed tissue-restricted markers, implying tissue-specific molding of ECs by the tissue micro-environment.

Fourth, we identified highly specialized EC phenotypes, such as *Madcam1*<sup>+</sup> vein ECs and *Aqp7*<sup>+</sup> capillary ECs in intestines and choroid plexus ECs in brain. It will, for instance, be interesting to explore whether future functional analysis validates *Madcam1*<sup>+</sup> vein ECs as HEV-like cells, involved in immune-cell recruitment to control immune homeostasis in gut. We also discovered *Aqp7*<sup>+</sup> capillary ECs in intestines. Because AQP7 is involved in glycerol and fatty-acid transport (Hibuse et al., 2006), an interesting question is whether *Aqp7*<sup>+</sup> ECs could represent a new alternative mechanism for removing glycerol from en-

terocytes into the portal system, bypassing the lacteal system. The presence of an interferon-activated EC phenotype in brain, muscle, heart, and spleen raises the question as to whether these ECs might be involved in immune surveillance. Emerging evidence suggests that hematopoietic cells as well as ECs control immune surveillance (Young, 2012).

Unexpectedly, we also identified the presence of angiogenic as well as proliferating ECs in otherwise healthy tissues, albeit at low numbers. Interestingly, at least some of these tissues (liver, spleen) exhibit a high regenerative potential after partial organ excision (Michalopoulos, 2010; Riera et al., 2009), relying partly on EC proliferation (Uda et al., 2013). Whether the low level of EC proliferation in some healthy tissues represents an ongoing EC repair/regeneration process remains to be further determined.

Fifth, as another phenotypic readout of our scRNA-seq analysis, we explored whether and to which extent ECs from different vascular beds in different tissues also exhibited heterogeneity of their metabolic transcriptome signature. The primary objective was not to make statements on metabolic fluxes but rather to characterize the metabolic gene-expression signatures, because the latter have been documented to be predictive in certain cases for cellular metabolism, at least at the bulk population level of ECs (Cantelmo et al., 2016; Marcu et al., 2018). When focusing on metabolic genes, EC heterogeneity was evident in ECs between tissues but also within a particular tissue.

ECs from brain/testis, splenic, pulmonary, and muscle/heart upregulated the expression of distinct sets of metabolic genes involved in a particular metabolic process (metabolite transport, cholesterol metabolism, cAMP metabolism/biosynthesis, and lipid uptake/metabolism, respectively). An additional level of EC heterogeneity was observed when analyzing the expression of metabolic genes in different vascular-bed compartments within a single tissue. A spectrum of different patterns was identified, ranging from upregulation of metabolic gene transcripts only in either arterial, capillary, venous, or lymphatic ECs or instead in each compartment of the vascular bed, or variations hereof, in a tissue-type-dependent pattern. These findings further illustrate the extensive phenotypic plasticity and potential of ECs to flexibly adapt their metabolic gene-expression signature, presumably to finetune their function to optimally respond to the physiological needs of each different tissue compartment.

Lastly, we demonstrated the usefulness of the EC Atlas taxonomy in annotating ECs in publicly available scRNA-seq datasets of murine tissues, thus providing not only a rich resource of molecular characteristics of different EC phenotypes in distinct tissues but also a powerful discovery tool to finetune the identification of ECs with unknown phenotype in other datasets.

This study also faces limitations. First, we only profiled 11 tissues, and only in mouse, thus offering future opportunities for an all-encompassing EC Atlas in all mouse and human tissues. Second, this study was not designed to study all types of lymphatic ECs in sufficient detail, though these cells seem to

(B) Dendrogram visualization of hierarchical clustering analysis of EC phenotypes assigned by scmap (using top 10 marker genes for each EC phenotype), derived from female (F) and male mice (M). Color differences in the dendrogram indicate subclusters, resolved by multiscale bootstrapping.  
 (C–E) Sankey diagrams, showing the scmap cluster projections of brain ECs from Vanlandewijck et al. (2018) (C), lung ECs from He et al. (2018) (D), and cardiac ECs from Zhao et al. (2018) (E) to the EC Atlas taxonomy. Similarity scores for each EC Atlas EC subcluster per tissue are shown in boxplots.

be transcriptomically stable across tissues. Third, we acknowledge that additional protein analysis and functional validation are required to confirm the putative role of each EC phenotype, that the assigned EC phenotypes are only based on transcriptomic data, that the predicted topographical localization of the EC subclusters alongside the vascular tree requires validation (for instance by spatial scRNA-seq methods), and that the tissue-grouping concept of ECs requires further corroboration. Finally, we cannot exclude the possibility that during dissociation of the tissues and FACS-based enrichment of ECs, certain cells or cell types were possibly lost. Nonetheless, this EC Atlas taxonomy in healthy conditions could facilitate the identification of EC phenotypes during pathological angiogenesis in cancer and eye disease, targets of current anti-angiogenic therapy.

## STAR★METHODS

Detailed methods are provided in the online version of this paper and include the following:

- KEY RESOURCES TABLE
- LEAD CONTACT AND MATERIALS AVAILABILITY
- EXPERIMENTAL MODEL AND SUBJECT DETAILS
  - Mice and Tissue Collection
- METHOD DETAILS
  - Tissue Dissociation And Sample Preparation
  - Library Preparation and Sequencing
  - Data Processing and *In Silico* EC Selection
  - Clustering of Tissues
  - Gene Set Analyses
  - Data Visualization
  - SCENIC
  - Comparison of Traditional EC Subtypes
  - Comparison of Tissue-Specialized EC Subtypes
  - Metabolic Gene Expression Analysis
  - Pseudotime
  - Analysis of Publicly Available EC Data
  - Immunohistochemistry
- QUANTIFICATION AND STATISTICAL ANALYSIS
- DATA AND CODE AVAILABILITY

## SUPPLEMENTAL INFORMATION

Supplemental Information can be found online at <https://doi.org/10.1016/j.cell.2020.01.015>.

## ACKNOWLEDGMENTS

We acknowledge the help of K. Peeters, A. Manderveld, A. Carton, J. Souffreau, C. De Legher, P. Vanwesemael, R. Schepers, and I.-M. Paulsen for assistance and D. Lambrechts, V. Lagani, T. Zheng, and J. Mulder for discussions. J.K., J.G., K.R., N.V.C., K.V., L.T., M.B., P.d.Z., and C.D. are supported by the Fonds voor Wetenschappelijk Onderzoek (FWO); J.K. by AIAS-COFUND II; GA: MSCA: 754513 and the Steno Diabetes Center Aarhus; L.-A.T. by University of Antwerp; V.G. by Strategisch Basisonderzoek Fonds voor Wetenschappelijk Onderzoek-Vlaanderen (SB-FWO); S.J.D. and K.D.F. by a Marie Curie-IEF Fellowship; S.K. by a grant from Kom op tegen Kanker (Stand up to Cancer, Flemish Cancer Society); L.L. by the Lundbeck Foundation (R219-2016-1375) and DFF Sapere Aude starting grant (8048-00072A); R.A.F. by the Novo Nordisk Foundation; L.B. and Y.L. by Sanming Project of Medicine in Shenzhen (SZSM201612074), BGI-Research, and Guangdong

Provincial Key Laboratory of Genome Read and Write (2017B030301011); X.L. by the State Key Laboratory of Ophthalmology, Zhongshan Ophthalmic Center (Sun Yat-Sen University), National Natural Science Foundation of China (81670855), and the Key Program of Guangzhou Scientific Research Plan (3030901006074); and P.C. by the VIB TechWatch program, Methusalem funding, FWO Vlaanderen, Foundation Against Cancer (2016-078), Kom op Tegen Kanker (Stand up to Cancer, Flemish Cancer Society), ERC Proof of Concept (ERC-713758), and an ERC Advanced Research Grant (EU-ERC743074).

## AUTHOR CONTRIBUTIONS

J.K. and L.d.R. designed and analyzed all experiments. J.K., L.d.R., J.G., K.R., F.T., and T.K.K. performed computational analysis. J.K., S.J.D., E.M., N.V.C., L.-A.T., K.V., M.G.C., V.G., R.C., L. Sokol., L.T., M.B., P.d.Z., C.D., K.D.F., and M.P. set up EC isolation protocols and performed EC isolations. L.L. and Y.L. performed 10x Genomics single-cell sequencing. S.K. processed scRNA-seq data. X.Y., Y.D., S.V., L. Schoonjans, M.D., G.E., R.A.F., B.T., L.L., L.B., X.L., and Y.L. provided reagents, advice, and discussed results. J.K., L.d.R., and P.C. wrote the manuscript. P.C. conceptualized the study. All authors discussed results and commented on the manuscript.

## DECLARATION OF INTERESTS

None of the authors have competing financial interests to declare.

Received: July 8, 2019

Revised: November 21, 2019

Accepted: January 9, 2020

Published: February 13, 2020

## REFERENCES

- Abraham, G., Qiu, Y., and Inouye, M. (2017). FlashPCA2: principal component analysis of Biobank-scale genotype datasets. *Bioinformatics* 33, 2776–2778.
- Abrahimi, P., Qin, L., Chang, W.G., Bothwell, A.L., Tellides, G., Saltzman, W.M., and Pober, J.S. (2016). Blocking MHC class II on human endothelium mitigates acute rejection. *JCI Insight* 1, e85293.
- Aibar, S., González-Blas, C.B., Moerman, T., Huynh-Thu, V.A., Imrichova, H., Hulselmans, G., Rambow, F., Marine, J.C., Geurts, P., Aerts, J., et al. (2017). SCENIC: single-cell regulatory network inference and clustering. *Nat. Methods* 14, 1083–1086.
- Asai, K., Kuzuya, M., Naito, M., Funaki, C., and Kuzuya, F. (1988). Effects of splenectomy on serum lipids and experimental atherosclerosis. *Angiology* 39, 497–504.
- Augustin, H.G., and Koh, G.Y. (2017). Organotypic vasculature: From descriptive heterogeneity to functional pathophysiology. *Science* 357, eaal2379.
- Baryawno, N., Przybylski, D., Kowalczyk, M.S., Kfoury, Y., Severe, N., Gustafsson, K., Kokkaliaris, K.D., Mercier, F., Tabaka, M., Hofree, M., et al. (2019). A Cellular Taxonomy of the Bone Marrow Stroma in Homeostasis and Leukemia. *Cell* 177, 1915–1932.e16.
- Bender, A.T., and Beavo, J.A. (2006). Cyclic nucleotide phosphodiesterases: molecular regulation to clinical use. *Pharmacol. Rev.* 58, 488–520.
- Bharadwaj, K.G., Hiyama, Y., Hu, Y., Huggins, L.A., Ramakrishnan, R., Abumrad, N.A., Shulman, G.I., Blaner, W.S., and Goldberg, I.J. (2010). Chylomicron- and VLDL-derived lipids enter the heart through different pathways: in vivo evidence for receptor- and non-receptor-mediated fatty acid uptake. *J. Biol. Chem.* 285, 37976–37986.
- Blum, J.S., Wearsch, P.A., and Cresswell, P. (2013). Pathways of antigen processing. *Annu. Rev. Immunol.* 31, 443–473.
- Bosma, E.K., van Noorden, C.J.F., Schlingemann, R.O., and Klaassen, I. (2018). The role of plasmalemma vesicle-associated protein in pathological breakdown of blood-brain and blood-retinal barriers: potential novel therapeutic target for cerebral edema and diabetic macular edema. *Fluids Barriers CNS* 15, 24.

- Bowyer, J.F., Patterson, T.A., Saini, U.T., Hanig, J.P., Thomas, M., Camacho, L., George, N.I., and Chen, J.J. (2013). Comparison of the global gene expression of choroid plexus and meninges and associated vasculature under control conditions and after pronounced hyperthermia or amphetamine toxicity. *BMC Genomics* 14, 147.
- Breitling, R., Armengaud, P., Amtmann, A., and Herzyk, P. (2004). Rank products: a simple, yet powerful, new method to detect differentially regulated genes in replicated microarray experiments. *FEBS Lett.* 573, 83–92.
- Bronte, V., and Pittet, M.J. (2013). The spleen in local and systemic regulation of immunity. *Immunity* 39, 806–818.
- Cannoodt, R., Saelens, W., Sichien, D., Tavernier, S., Janssens, S., Guillemins, M., Lambrecht, B., Preter, K.D., and Saeys, Y. (2016). SCORPIUS improves trajectory inference and identifies novel modules in dendritic cell development. *bioRxiv*, 079509.
- Cantelmo, A.R., Conradi, L.C., Brajic, A., Goveia, J., Kalucka, J., Pircher, A., Chaturvedi, P., Hol, J., Thienpont, B., Teuwen, L.A., et al. (2016). Inhibition of the Glycolytic Activator PFKFB3 in Endothelium Induces Tumor Vessel Normalization, Impairs Metastasis, and Improves Chemotherapy. *Cancer Cell* 30, 968–985.
- Chen, H., and Boutros, P.C. (2011). VennDiagram: a package for the generation of highly-customizable Venn and Euler diagrams in R. *BMC Bioinformatics* 12, 35.
- Conway, J.R., Lex, A., and Gehlenborg, N. (2017). UpSetR: an R package for the visualization of intersecting sets and their properties. *Bioinformatics* 33, 2938–2940.
- Daneman, R., and Rescigno, M. (2009). The gut immune barrier and the blood-brain barrier: are they so different? *Immunity* 31, 722–735.
- Divine, J.K., Staloch, L.J., Haveri, H., Jacobsen, C.M., Wilson, D.B., Heikinheimo, M., and Simon, T.C. (2004). GATA-4, GATA-5, and GATA-6 activate the rat liver fatty acid binding protein gene in concert with HNF-1alpha. *Am. J. Physiol. Gastrointest. Liver Physiol.* 287, G1086–G1099.
- Dixon, J.B. (2010). Mechanisms of chylomicron uptake into lacteals. *Ann. N Y Acad. Sci.* 1207 (Suppl 1), E52–E57.
- Doenst, T., Nguyen, T.D., and Abel, E.D. (2013). Cardiac metabolism in heart failure: implications beyond ATP production. *Circ. Res.* 113, 709–724.
- Dumas, S.J., Meta, E., Borri, M., Goveia, J., Rohlenova, K., Conchinha, N.V., Falkenberg, K., Teuwen, L.A., de Rooij, L., Kalucka, J., et al. (2020). Single-Cell RNA Sequencing Reveals Renal Endothelium Heterogeneity and Metabolic Adaptation to Water Deprivation. *J. Am. Soc. Nephrol.* 31, 118–138.
- Falkenberg, K.R.K., Luo, Y., and Carmeliet, P. (2019). The metabolic engine of endothelial cells. *Nature Metabolism*, 937–946.
- Fischer, A., Schumacher, N., Maier, M., Sendtner, M., and Gessler, M. (2004). The Notch target genes Hey1 and Hey2 are required for embryonic vascular development. *Genes Dev.* 18, 901–911.
- Fraser, J.R., Laurent, T.C., and Laurent, U.B. (1997). Hyaluronan: its nature, distribution, functions and turnover. *J. Intern. Med.* 242, 27–33.
- Galili, T., O'Callaghan, A., Sidi, J., and Sievert, C. (2018). heatmaply: an R package for creating interactive cluster heatmaps for online publishing. *Bioinformatics* 34, 1600–1602.
- Ghazdour, M.S., Langley, O.K., Zhu, X.L., Waheed, A., and Sly, W.S. (1992). Carbonic anhydrase IV on brain capillary endothelial cells: a marker associated with the blood-brain barrier. *Proc. Natl. Acad. Sci. USA* 89, 6823–6827.
- Girard, J.P., Moussion, C., and Förster, R. (2012). HEVs, lymphatics and homeostatic immune cell trafficking in lymph nodes. *Nat. Rev. Immunol.* 12, 762–773.
- Goveia, J., Rohlenova, K., Taverna, F., Treps, L., Conradi, L.C., Pircher, A., Geldhof, V., de Rooij, L., Kalucka, J., Sokol, L., et al. (2020). An Integrated Gene Expression Landscape Profiling Approach to Identify Lung Tumor Endothelial Cell Heterogeneity and Angiogenic Candidates. *Cancer Cell* 37, 21–36.e13.
- Gustavsson, C., Agardh, C.D., Zetterqvist, A.V., Nilsson, J., Agardh, E., and Gomez, M.F. (2010). Vascular cellular adhesion molecule-1 (VCAM-1) expression in mice retinal vessels is affected by both hyperglycemia and hyperlipidemia. *PLoS ONE* 5, e12699.
- Han, X., Wang, R., Zhou, Y., Fei, L., Sun, H., Lai, S., Saadatpour, A., Zhou, Z., Chen, H., Ye, F., et al. (2018). Mapping the Mouse Cell Atlas by Microwell-Seq. *Cell* 172, 1091–1107.e17.
- Hänelmann, S., Castelo, R., and Guinney, J. (2013). GSVA: gene set variation analysis for microarray and RNA-seq data. *BMC Bioinformatics* 14, 7.
- He, L., Vanlandewijck, M., Mäe, M.A., Andrae, J., Ando, K., Del Gaudio, F., Nahar, K., Lebouvier, T., Laviña, B., Gouveia, L., et al. (2018). Single-cell RNA sequencing of mouse brain and lung vascular and vessel-associated cell types. *Sci. Data* 5, 180160.
- Heskes, T., Eisinga, R., and Breitling, R. (2014). A fast algorithm for determining bounds and accurate approximate p-values of the rank product statistic for replicate experiments. *BMC Bioinformatics* 15, 367.
- Hibuse, T., Maeda, N., Nagasawa, A., and Funahashi, T. (2006). Aquaporins and glycerol metabolism. *Biochim. Biophys. Acta* 1758, 1004–1011.
- Iso, T., Maeda, K., Hanaoka, H., Suga, T., Goto, K., Syamsunarno, M.R., Hishiki, T., Nagahata, Y., Matsui, H., Arai, M., et al. (2013). Capillary endothelial fatty acid binding proteins 4 and 5 play a critical role in fatty acid uptake in heart and skeletal muscle. *Arterioscler. Thromb. Vasc. Biol.* 33, 2549–2557.
- Jourde-Chiche, N., Fakhouri, F., Dou, L., Bellien, J., Burtey, S., Frimat, M., Jarrot, P.A., Kaplanski, G., Le Quintrec, M., Pernin, V., et al. (2019). Endothelium structure and function in kidney health and disease. *Nat. Rev. Nephrol.* 15, 87–108.
- Kamitani, S., Asakawa, M., Shimekake, Y., Kuwasako, K., Nakahara, K., and Sakata, T. (1999). The RAMP2/CRLR complex is a functional adrenomedullin receptor in human endothelial and vascular smooth muscle cells. *FEBS Lett.* 448, 111–114.
- Kanai, Y., Segawa, H., Miyamoto, Ki., Uchino, H., Takeda, E., and Endou, H. (1998). Expression cloning and characterization of a transporter for large neutral amino acids activated by the heavy chain of 4F2 antigen (CD98). *J. Biol. Chem.* 273, 23629–23632.
- Kashiwazaki, M., Tanaka, T., Kanda, H., Ebisuno, Y., Izawa, D., Fukuma, N., Akimitsu, N., Sekimizu, K., Monden, M., and Miyasaka, M. (2003). A high endothelial venule-expressing promiscuous chemokine receptor DARC can bind inflammatory, but not lymphoid, chemokines and is dispensable for lymphocyte homing under physiological conditions. *Int. Immunol.* 15, 1219–1227.
- Khan, S., Taverna, F., Rohlenova, K., Treps, L., Geldhof, V., de Rooij, L., Sokol, L., Pircher, A., Conradi, L.C., Kalucka, J., et al. (2019). EndoDB: a database of endothelial cell transcriptomics data. *Nucleic Acids Res.* 47 (D1), D736–D744.
- Kiselev, V.Y., Yiu, A., and Hemberg, M. (2018). scmap: projection of single-cell RNA-seq data across data sets. *Nat. Methods* 15, 359–362.
- Lee, S., Chen, T.T., Barber, C.L., Jordan, M.C., Murdock, J., Desai, S., Ferrara, N., Nagy, A., Roos, K.P., and Iruela-Arispe, M.L. (2007). Autocrine VEGF signaling is required for vascular homeostasis. *Cell* 130, 691–703.
- Li, X., Sun, X., and Carmeliet, P. (2019). Hallmarks of Endothelial Cell Metabolism in Health and Disease. *Cell Metab.* 30, 414–433.
- Lukowski, S.W., Patel, J., Andersen, S.B., Sim, S.L., Wong, H.Y., Tay, J., Winkler, I., Powell, J.E., and Khosrotehrani, K. (2019). Single-Cell Transcriptional Profiling of Aortic Endothelium Identifies a Hierarchy from Endovascular Progenitors to Differentiated Cells. *Cell Rep.* 27, 2748–2758.e3.
- Mai, J., Virtue, A., Shen, J., Wang, H., and Yang, X.F. (2013). An evolving new paradigm: endothelial cells–conditional innate immune cells. *J. Hematol. Oncol.* 6, 61.
- Marcu, R., Choi, Y.J., Xue, J., Fortin, C.L., Wang, Y., Nagao, R.J., Xu, J., MacDonald, J.W., Bammier, T.K., Murry, C.E., et al. (2018). Human Organ-Specific Endothelial Cell Heterogeneity. *iScience* 4, 20–35.
- Martinu, T., Chen, D.F., and Palmer, S.M. (2009). Acute rejection and humoral sensitization in lung transplant recipients. *Proc. Am. Thorac. Soc.* 6, 54–65.
- McInnes, L., Healy, J., and Melville, J. (2018). UMAP: Uniform Manifold Approximation and Projection for Dimension Reduction. *arXiv:180203426*.

- Michalopoulos, G.K. (2010). Liver regeneration after partial hepatectomy: critical analysis of mechanistic dilemmas. *Am. J. Pathol.* **176**, 2–13.
- Murakami, M., Nguyen, L.T., Zhuang, Z.W., Moodie, K.L., Carmeliet, P., Stan, R.V., and Simons, M. (2008). The FGF system has a key role in regulating vascular integrity. *J. Clin. Invest.* **118**, 3355–3366.
- Muramatsu, T., and Miyauchi, T. (2003). Basigin (CD147): a multifunctional transmembrane protein involved in reproduction, neural function, inflammation and tumor invasion. *Histol. Histopathol.* **18**, 981–987.
- Nejsum, L.N., Elkjaer, M., Hager, H., Frokiaer, J., Kwon, T.H., and Nielsen, S. (2000). Localization of aquaporin-7 in rat and mouse kidney using RT-PCR, immunoblotting, and immunocytochemistry. *Biochem. Biophys. Res. Commun.* **277**, 164–170.
- Nolan, D.J., Ginsberg, M., Israely, E., Palikuqi, B., Poulos, M.G., James, D., Ding, B.S., Schachterle, W., Liu, Y., Rosenwaks, Z., et al. (2013). Molecular signatures of tissue-specific microvascular endothelial cell heterogeneity in organ maintenance and regeneration. *Dev. Cell* **26**, 204–219.
- Park, J., Shrestha, R., Qiu, C., Kondo, A., Huang, S., Werth, M., Li, M., Barasch, J., and Suszták, K. (2018). Single-cell transcriptomics of the mouse kidney reveals potential cellular targets of kidney disease. *Science* **360**, 758–763.
- Poisson, J., Lemoinne, S., Boulanger, C., Durand, F., Moreau, R., Valla, D., and Rautou, P.E. (2017). Liver sinusoidal endothelial cells: Physiology and role in liver diseases. *J. Hepatol.* **66**, 212–227.
- Potente, M., and Mäkinen, T. (2017). Vascular heterogeneity and specialization in development and disease. *Nat. Rev. Mol. Cell Biol.* **18**, 477–494.
- Pusztaszteri, M.P., Seelentag, W., and Bosman, F.T. (2006). Immunohistochemical expression of endothelial markers CD31, CD34, von Willebrand factor, and Flt-1 in normal human tissues. *J. Histochem. Cytochem.* **54**, 385–395.
- Qiu, J., Salama, M.E., Hu, C.S., Li, Y., Wang, X., and Hoffman, R. (2018). The characteristics of vessel lining cells in normal spleens and their role in the pathobiology of myelofibrosis. *Blood Adv.* **2**, 1130–1145.
- Riera, M., Buczacki, S., and Khan, Z.A. (2009). Splenic regeneration following splenectomy and impact on sepsis: a clinical review. *J. R. Soc. Med.* **102**, 139–142.
- Ritchie, M.E., Phipson, B., Wu, D., Hu, Y., Law, C.W., Shi, W., and Smyth, G.K. (2015). limma powers differential expression analyses for RNA-sequencing and microarray studies. *Nucleic Acids Res.* **43**, e47.
- Sabbagh, M.F., Heng, J.S., Luo, C., Castanon, R.G., Nery, J.R., Rattner, A., Goff, L.A., Ecker, J.R., and Nathans, J. (2018). Transcriptional and epigenomic landscapes of CNS and non-CNS vascular endothelial cells. *eLife* **7**, 7.
- Sahoo, S., Aurich, M.K., Jonsson, J.J., and Thiele, I. (2014). Membrane transporters in a human genome-scale metabolic knowledgebase and their implications for disease. *Front. Physiol.* **5**, 91.
- Saito, K., Tanaka, T., Kanda, H., Ebisuno, Y., Izawa, D., Kawamoto, S., Okubo, K., and Miyasaka, M. (2002). Gene expression profiling of mucosal addressin cell adhesion molecule-1+ high endothelial venules (HEV) and identification of a leucine-rich HEV glycoprotein as a HEV marker. *J. Immunol.* **168**, 1050–1059.
- Satija, R., Farrell, J.A., Gennert, D., Schier, A.F., and Regev, A. (2015). Spatial reconstruction of single-cell gene expression data. *Nat. Biotechnol.* **33**, 495–502.
- Sayner, S.L. (2011). Emerging themes of cAMP regulation of the pulmonary endothelial barrier. *Am. J. Physiol. Lung Cell. Mol. Physiol.* **300**, L667–L678.
- Seternes, T., Sørensen, K., and Smedsrød, B. (2002). Scavenger endothelial cells of vertebrates: a nonperipheral leukocyte system for high-capacity elimination of waste macromolecules. *Proc. Natl. Acad. Sci. USA* **99**, 7594–7597.
- Sharpe, L.J., and Brown, A.J. (2013). Controlling cholesterol synthesis beyond 3-hydroxy-3-methylglutaryl-CoA reductase (HMGCR). *J. Biol. Chem.* **288**, 18707–18715.
- Shetty, S., Lalor, P.F., and Adams, D.H. (2018). Liver sinusoidal endothelial cells - gatekeepers of hepatic immunity. *Nat. Rev. Gastroenterol. Hepatol.* **15**, 555–567.
- Skowronski, M.T., Lebeck, J., Rojek, A., Praetorius, J., Füchtbauer, E.M., Frokiaer, J., and Nielsen, S. (2007). AQP7 is localized in capillaries of adipose tissue, cardiac and striated muscle: implications in glycerol metabolism. *Am. J. Physiol. Renal Physiol.* **292**, F956–F965.
- Spadoni, I., Zagato, E., Bertocchi, A., Paolinelli, R., Hot, E., Di Sabatino, A., Caprioli, F., Bottiglieri, L., Oldani, A., Viale, G., et al. (2015). A gut-vascular barrier controls the systemic dissemination of bacteria. *Science* **350**, 830–834.
- Storey, J.D., Bass, A.J., Dabney, A., and Robinson, D. (2015). qvalue: Q-value estimation for false discovery rate control. R package version 2.100. <http://github.com/jdstorey/qvalue>.
- Su, L., Mruk, D.D., and Cheng, C.Y. (2011). Drug transporters, the blood-testis barrier, and spermatogenesis. *J. Endocrinol.* **208**, 207–223.
- Su, T., Stanley, G., Sinha, R., D'Amato, G., Das, S., Rhee, S., Chang, A.H., Poduri, A., Raftrey, B., Dinh, T.T., et al. (2018). Single-cell analysis of early progenitor cells that build coronary arteries. *Nature* **559**, 356–362.
- Suzuki, R., and Shimodaira, H. (2006). Pvclust: an R package for assessing the uncertainty in hierarchical clustering. *Bioinformatics* **22**, 1540–1542.
- Sweeney, M.D., Sagare, A.P., and Zlokovic, B.V. (2018). Blood-brain barrier breakdown in Alzheimer disease and other neurodegenerative disorders. *Nat. Rev. Neurol.* **14**, 133–150.
- Sweeney, M.D., Zhao, Z., Montagne, A., Nelson, A.R., and Zlokovic, B.V. (2019). Blood-Brain Barrier: From Physiology to Disease and Back. *Physiol. Rev.* **99**, 21–78.
- Tabula Muris Consortium; Overall coordination; Logistical coordination; Organ collection and processing; Library preparation and sequencing; Computational data analysis; Cell type annotation; Writing group; Supplemental text writing group; Principal investigators (2018). Single-cell transcriptomics of 20 mouse organs creates a Tabula Muris. *Nature* **562**, 367–372.
- Tikhonova, A.N., Dolgalev, I., Hu, H., Sivaraj, K.K., Hoxha, E., Cuesta-Domínguez, A., Pinho, S., Akhmetzyanova, I., Gao, J., Witkowski, M., et al. (2019). The bone marrow microenvironment at single-cell resolution. *Nature* **569**, 222–228.
- Uda, Y., Hirano, T., Son, G., Iimuro, Y., Uyama, N., Yamanaka, J., Mori, A., Arii, S., and Fujimoto, J. (2013). Angiogenesis is crucial for liver regeneration after partial hepatectomy. *Surgery* **153**, 70–77.
- van den Brink, S.C., Sage, F., Vértesy, Á., Spanjaard, B., Peterson-Maduro, J., Baron, C.S., Robin, C., and van Oudenaarden, A. (2017). Single-cell sequencing reveals dissociation-induced gene expression in tissue subpopulations. *Nat. Methods* **14**, 935–936.
- van der Maaten, L.J.P., and Hinton, G.E. (2008). Visualizing High-Dimensional Data Using t-SNE. *J. Mach. Learn. Res.* **9**, 2579–2605.
- Vanlandewijck, M., He, L., Mæe, M.A., Andrae, J., Ando, K., Del Gaudio, F., Nahar, K., Lebouvier, T., Laviña, B., Gouveia, L., et al. (2018). A molecular atlas of cell types and zonation in the brain vasculature. *Nature* **554**, 475–480.
- Watt, M.J., and Hoy, A.J. (2012). Lipid metabolism in skeletal muscle: generation of adaptive and maladaptive intracellular signals for cellular function. *Am. J. Physiol. Endocrinol. Metab.* **302**, E1315–E1328.
- Watt, A.J., Zhao, R., Li, J., and Duncan, S.A. (2007). Development of the mammalian liver and ventral pancreas is dependent on GATA4. *BMC Dev. Biol.* **7**, 37.
- Wohlleber, D., and Knolle, P.A. (2016). The role of liver sinusoidal cells in local hepatic immune surveillance. *Clin. Transl. Immunology* **5**, e117.
- Young, M.R. (2012). Endothelial cells in the eyes of an immunologist. *Cancer Immunol. Immunother.* **61**, 1609–1616.
- Zhao, Q., Eichten, A., Parveen, A., Adler, C., Huang, Y., Wang, W., Ding, Y., Adler, A., Nevins, T., Ni, M., et al. (2018). Single-Cell Transcriptome Analyses Reveal Endothelial Cell Heterogeneity in Tumors and Changes following Anti-angiogenic Treatment. *Cancer Res.* **78**, 2370–2382.

## STAR★METHODS

## KEY RESOURCES TABLE

REAGENT or RESOURCE	SOURCE	IDENTIFIER
<b>Antibodies</b>		
Rat anti-mouse/human CD11b-PE (clone M1/70)	BioLegend	Cat#101208; RRID: AB_312791
Rat anti-mouse CD31 FITC (clone 390)	Thermo Fisher Scientific	Cat#11-0311-85; RRID: AB_465012
Rat anti-mouse CD45 PE-Cy7 (clone 30-F11)	Thermo Fisher Scientific	Cat#25-0451-82; RRID: AB_2734986
Goat anti-mouse CD105	R&D	Cat#AF1320; RRID: AB_354735
Rat anti-mouse MAdCAM1 (clone AP-MAB0842)	Abcam	Cat#ab80860; RRID: AB_1640676
Rabbit anti-mouse ISG15	Thermo Fisher Scientific	Cat#PA5-79523; RRID: AB_2746639
Rabbit anti-mouse Ki67 (clone SP6)	Thermo Fisher Scientific	Cat#MA5-14520; RRID: AB_10979488
Goat anti-mouse ESM1	R&D	Cat#AF1999; RRID: AB_2101810
Rat anti-mouse CD31 (clone MEC13.3)	BD Biosciences	Cat#550274; RRID: AB_393571
Rat anti-PLVAP	DHSB	Cat#MECA-32; RRID: AB_531797
Mouse anti-SMA Cy3 (clone 1A4)	Sigma-Aldrich	Cat#C6198; RRID: AB_476856
Rabbit anti-AQP7	<a href="#">Nejsum et al., 2000</a>	N/A
Prolong Gold Antifade Mountant	Thermo Fisher Scientific	Cat#P36934
<b>Chemicals, Peptides, and Recombinant Proteins</b>		
Dithiothreitol (DTT)	Sigma-Aldrich,	Cat#10197777001
DMSO	Sigma-Aldrich	Cat#D2438
DNase I	Sigma-Aldrich	Cat#D4527-10KU
Ficoll-Paque	GE Life Sciences	Cat#17144002
EDTA	Thermo Fisher Scientific	Cat#14190-094
Sodium pyruvate	Thermo Fisher Scientific	Cat#1360070
Viable dye eFluor 450	Thermo Fisher Scientific	Cat#65-0863-18
<b>Critical Commercial Assays</b>		
CD31 MicroBeads, mouse	Miltenyi Biotec	Cat#130-097-418
CD45 MicroBeads, mouse	Miltenyi Biotec	Cat#130-052-301
EpCAM MicroBeads, mouse	Miltenyi Biotec	Cat#130-105-958
Chromium Single Cell 3' Library, Gel Bead & Multiplex Kit and Chip Kit, v2	10x Genomics	PN-120237
Chromium Single Cell A Chip Kit	10x Genomics	PN-120236
Chromium i7 Multiplex Kit	10x Genomics	PN-120262
Neural Tissue Dissociation kit (P)	Miltenyi Biotec	Cat#130-096-733
Myelin Removal Beads II	Miltenyi Biotec	Cat#130-096-733
TSA Cyanine 3 (Cy3) System	Perkin Elmer	NEL704A001KT
TSA Cyanine 5 (Cy5) System	Perkin Elmer	NEL705A001KT
TSA Fluorescein System	Perkin Elmer	NEL701A001KT
<b>Deposited Data</b>		
RNA-sequencing raw and analyzed data mouse EC	This paper	ArrayExpress: E-MTAB-8077
<b>Experimental Models: Organisms/Strains</b>		
C57BL/6J mice	Charles River	N/A
<b>Software and Algorithms</b>		
R version 3.4.4 system: x86_64, mingw32	The R Foundation	<a href="https://www.r-project.org">https://www.r-project.org</a>
ui: RStudio (1.1.456) language: (EN) collate: English United States.1252	Open source	<a href="https://rstudio.com">https://rstudio.com</a>

(Continued on next page)

***Continued***

REAGENT or RESOURCE	SOURCE	IDENTIFIER
Cell Ranger; version 2.2.0	10x Genomics	(tenx; RRID: SCR_01695)
flashpcaR; version 2.0	Abraham et al., 2017	<a href="https://github.com/gabraham/flashpca/releases">https://github.com/gabraham/flashpca/releases</a>
GSVA; version 1.26.0	Hänelmann et al., 2013	<a href="http://bioconductor.statistik.tu-dortmund.de/packages/3.6/bioc/html/GSVA.html">http://bioconductor.statistik.tu-dortmund.de/packages/3.6/bioc/html/GSVA.html</a>
heatmaply; version 0.16.0	Galili et al., 2018	<a href="https://cran.r-project.org/src/contrib/Archive/heatmaply/">https://cran.r-project.org/src/contrib/Archive/heatmaply/</a>
limma; version 3.34.9	Ritchie et al., 2015	(LIMMA; RRID: SCR_010943)
plotly; version 4.8.0.9000	Github (ropensci/plotly@f43699e)	(plotly; RRID: SCR_013991)
Rtsne; version 0.15	van der Maaten and Hinton, 2008	<a href="https://CRAN.R-project.org/package=Rtsne">https://CRAN.R-project.org/package=Rtsne</a>
umap: version 0.2.0.0	McInnes et al., 2018	<a href="https://cran.r-project.org/src/contrib/Archive/umap/">https://cran.r-project.org/src/contrib/Archive/umap/</a>
pvclust: version 2.0.0	Suzuki and Shimodaira, 2006	<a href="https://cran.r-project.org/src/contrib/Archive/pvclust/">https://cran.r-project.org/src/contrib/Archive/pvclust/</a>
qvalue: version 2.10.0	Storey et al., 2015	<a href="http://github.com/jdstorey/qvalue">http://github.com/jdstorey/qvalue</a>
org.Mm.eg.db: version 3.5.0	Bioconductor	<a href="http://bioconductor.org/packages/release/data/annotation/html/org.Mm.eg.db.html">http://bioconductor.org/packages/release/data/annotation/html/org.Mm.eg.db.html</a>
SCENIC; version 1.1.0	Aibar et al., 2017	<a href="https://aertslab.org/#scenic">https://aertslab.org/#scenic</a>
scmap; version 1.1.5	Kiselev et al., 2018	(scmap; RRID: SCR_017338)
Seurat; version 2.3.4	Satija et al., 2015	(Seurat; RRID: SCR_016341)
UpSetR; version 1.3.3	Conway et al., 2017	<a href="https://cran.r-project.org/src/contrib/Archive/UpSetR/">https://cran.r-project.org/src/contrib/Archive/UpSetR/</a>
VennDiagram; version 1.6.20	Chen and Boutros, 2011	(VennDiagram; RRID: SCR_002414)
SCORPIUS; version 1.0.2	Cannoodt et al., 2016	<a href="https://cran.r-project.org/src/contrib/Archive/SCORPIUS/">https://cran.r-project.org/src/contrib/Archive/SCORPIUS/</a>
GraphPad Prism8, version 8.1.1	Graphpad	(GraphPad Prism; RRID: SCR_002798)
Fiji (ImageJ)	Open source	<a href="https://fiji.sc">https://fiji.sc</a>
Other		
Antibiotic-antimycotic	Thermo Fisher Scientific	Cat#15240062
Bovine serum albumin (BSA Fraction V)	Sigma-Aldrich	Cat#10735096001
40 µm cell strainer	Sigma-Aldrich	Cat#CLS431750-50EA
70 µm cell strainer	Sigma-Aldrich	Cat#CLS431751-50EA
100 µm cell strainer	Sigma-Aldrich	Cat#CLS431752-50EA
Collagenase type I	Sigma-Aldrich	Cat#C9891
Collagenase type I	Thermo Fisher Scientific	Cat#17018029
Collagenase type II	Thermo Fisher Scientific	Cat#17101015
Collagenase type IV	Worthington Biochemical	Cat#LS004188
DMEM	Thermo Fisher Scientific	Cat# 11965092
Dispase	Thermo Fisher Scientific	Cat#171055-041
Fetal bovine serum (FBS)	Thermo Fisher Scientific	Cat#A38401
GentleMACS C tubes	Miltenyi Biotec	Cat#130-093-237
Glass Pasteur pipette with narrow tip	VWR	Cat#612-3813
Hank's Balanced Salt Solution (HBSS)	Thermo Fisher Scientific	Cat#14025092
Nimtek (100mg/mL); Ketamine	Dechra	N/A
KnockOut™ DMEM	Thermo Fisher Scientific	Cat#10829018
LD columns	Miltenyi Biotec	Cat#130-042-901
MEM NEAA	Thermo Fisher Scientific	Cat#11140035
Penicillin/streptomycin	Thermo Fisher Scientific	Cat#15140122
Phosphate buffered saline (PBS)	Thermo Fisher Scientific	Cat#14190-094
Xylazine, XYL-M 2%	V.M.D.	BE-V170581

## LEAD CONTACT AND MATERIALS AVAILABILITY

Correspondence and requests for materials should be addressed to the Lead Contact, Peter Carmeliet ([peter.carmeliet@kuleuven.vib.be](mailto:peter.carmeliet@kuleuven.vib.be)). This study did not generate new unique reagents.

## EXPERIMENTAL MODEL AND SUBJECT DETAILS

### Mice and Tissue Collection

Experiments were performed in 8-week-old male C57BL6/J mice (purchased from Charles Rivers). Mice were housed in the experimental animal lab for no longer than 2 weeks before euthanasia. To optimally standardize EC isolations, we isolated ECs from different tissues on the same day, as indicated below. The isolation procedures were performed over the course of 4 days and a total number of 30 male mice was used. Since the yield of ECs differed between tissues, we generally isolated tissues from 8 mice, except for the lung, liver, kidney and heart, where 6 mice sufficed to obtain the required number of ECs for further downstream analysis. No strategy for randomization or stratification was needed, nor blinding at any stage of the study. Inclusion and exclusion criteria of data are indicated in the sections describing the data processing and analysis in [Method Details](#). Strategy for EC isolation: Day 1, isolation of lung, heart and brain ECs. Day 2, isolation of testis and small intestine ECs. Day 3, isolation of liver and kidney ECs. Day 4, isolation of EDL, soleus, colon and spleen ECs. After anesthesia with ketamine (0.9%)/xylazine (2%), mice were weighed before transcardial perfusion with ice-cold PBS, followed by perfusion with the digestion buffer containing KnockOut<sup>TM</sup> DMEM (Thermo Fisher Scientific, Cat#10829018), 1% penicillin/streptomycin (Thermo Fisher Scientific, Cat#15140122), 2x Antibiotic-Antimycotic (Thermo Fisher Scientific, Cat#15240062), 1 mM sodium pyruvate (Thermo Fisher Scientific, Cat#1360070), 1x MEM Non-Essential Amino Acids Solution (Thermo Fisher Scientific, Cat#11140035) and supplemented with 0.1% collagenase I (Thermo Fisher Scientific, Cat#17018029), 0.1% collagenase II (Thermo Fisher Scientific, Cat#17101015) and 7.5 µg/mL DNase I (Sigma-Aldrich, Cat#D4527-10KU) at a perfusion rate of 2 mL/minute. Most of the individual tissues were digested separately. However, to ensure efficient digestion and to prevent excessive cell loss, testis, heart, extensor digitorum longus, soleus and spleen were pooled at this step (per 2-3 mice). After tissue dissociation (as described for each organ below), enrichment for CD31<sup>+</sup> cells and staining with various anti-body combinations for multi-parameter flow acquisition was performed. Cell suspensions were filtered using Falcon® Round-Bottom Tubes with Cell Strainer Cap (STEMCELL Technologies, Cat#38030) before performing FACS sorting on an Aria III (BD Bioscience). Animal housing and all experimental procedures were approved by the Institutional Animal Ethics Committee of the KU Leuven (Belgium) under protocol number P012/2018.

## METHOD DETAILS

### Tissue Dissociation And Sample Preparation

#### **Brain ECs**

After perfusion, the brain was surgically removed and placed in ice-cold Dulbecco's modified Eagle's medium (DMEM, Thermo Fisher Scientific) supplemented with 1x penicillin/streptomycin (Thermo Fisher Scientific, Cat#15140122). For all brain single-cell isolations, the entire brain (without olfactory bulb) was used. A single brain was transferred to a chilled Petri Dish on ice and minced with a scalpel. Next, brain ECs were isolated with a modified version of the Neural Tissue Dissociation kit (P) (Miltenyi Biotec, Cat#130-092-628), which allows mechanical and enzymatic dissociation of brain tissue before removal of myelin, which is detrimental for efficient sorting. Myelin was removed using magnetic bead separation (Myelin Removal Beads II, Miltenyi Biotec, Cat#130-096-733). The single cell suspension was enriched for ECs using CD31 MicroBeads (Miltenyi Biotec, Cat#130-097-418) according to the manufacturer's instructions. The CD31 enriched single cell suspension was washed with a PBS-based wash buffer (WB; containing 0.5% BSA (BSA Fraction V, Sigma-Aldrich, Cat#10735096001), 2 mM EDTA in PBS (Thermo Fisher Scientific, Cat#14190-094)) and stained with CD45-PE-Cy7 (clone 30-F11; Thermo Fisher Scientific, Cat#25-0451-82); CD31-FITC (clone 390; Thermo Fisher Scientific, Cat#11-0311-85) and Viable dye eFluor 450 (Thermo Fisher Scientific, Cat#65-0863-18). Doublets were gated out prior to FACS sorting. Viable CD45<sup>-</sup> CD31<sup>+</sup> ECs were sorted into collecting medium (10% FBS, Thermo Fisher Scientific, Cat#A38401).

#### **Lung ECs**

After perfusion, the lungs were surgically removed, rinsed in ice-cold PBS and lobes were separated. All lobes from one animal were transferred into a gentleMACS C tube (Miltenyi Biotec, Cat#130-096-334) containing digestion medium (KnockOut<sup>TM</sup> DMEM (Thermo Fisher Scientific, Cat#10829018); penicillin/streptomycin (Thermo Fisher Scientific, Cat#15140122); 2x Antibiotic-Antimycotic, (Thermo Fisher Scientific, Cat#15240062); 1 mM sodium pyruvate (Thermo Fisher Scientific, Cat#1360070); 1x MEM Non-Essential Amino Acids Solution (Thermo Fisher Scientific, Cat#11140035) supplemented with 0.1% collagenase II (Thermo Fisher Scientific, Cat#17101015); 0.25% collagenase IV (Worthington, Cat#LS004188) and 15 µg/mL DNase I (Sigma-Aldrich, #D4527-10KU)). Each sample was further dissociated using the gentle MACS dissociator system (MACS Technology, Miltenyi Biotec). First, samples were run using the m\_lung\_01 protocol (pre-programmed by the manufacturer) and then the samples were placed in a HulaMixer rotator (12 rpm) (Thermo Fisher Scientific, Cat# 15920D) at 37°C for 30 min. At the end of the incubation time, samples were again processed using the MACS dissociator system using the m\_lung\_02 protocol (pre-programmed by manufacturer). The cell suspension was filtered through a 40 µm cell strainer (Sigma-Aldrich, Cat# CLS431750-50EA) and the cell strainer was rinsed with a

PBS-based wash buffer (WB; containing 0.5% BSA (BSA Fraction V, Sigma-Aldrich, Cat#10735096001), 2 mM EDTA in PBS (Thermo Fisher Scientific, Cat#14190-094)). The cell suspension was then centrifuged at 200 g for 5 min. The washing steps were repeated twice. Next, the cell suspension was depleted of CD45<sup>+</sup> and EpCAM<sup>+</sup> cells using CD45 (MACS Technology, Miltenyi Biotec, Cat #130-052-301) and EpCAM (MACS Technology, Miltenyi Biotec, Cat #130-105-958) MicroBeads, according to the manufacturer's instructions. Next, the obtained CD45 and EpCAM depleted single cell suspension was enriched for ECs using CD31 MicroBeads (Miltenyi Biotec, Cat#130-097-418) according to the manufacturer's instructions. The CD31 enriched single cell suspension was washed with WB and stained with CD45-PE-Cy7 (clone 30-F11 Thermo Fisher Scientific, Cat#25-0451-82); CD31-FITC (clone 390; Thermo Fisher Scientific, Cat#11-0311-85) and Viable dye eFluor 450 (Thermo Fisher Scientific, Cat#65-0863-18). Doublets were gated out prior to FACS sorting. Viable, CD45<sup>-</sup> CD31<sup>+</sup> ECs were sorted into collecting medium (10% FBS, Thermo Fisher Scientific, Cat#A38401).

#### **Heart ECs**

After perfusion, the heart was surgically removed, rinsed with ice-cold PBS and dissected into small pieces using sterile scalpels. All pieces from one animal were transferred into a gentleMACS C tube (Miltenyi Biotec, Cat#130-096-334) containing digestion medium (KnockOut™ DMEM (Thermo Fisher Scientific, Cat#10829018); 1x penicillin/streptomycin (Thermo Fisher Scientific, Cat#15140122); 2x Antibiotic-Antimycotic (Thermo Fisher Scientific, Cat#15240062); 1 mM sodium pyruvate (Thermo Fisher Scientific, Cat#1360070); 1x MEM Non-Essential Amino Acids Solution (Thermo Fisher Scientific, Cat#11140035) supplemented with 0.1% collagenase II (Thermo Fisher Scientific, Cat#17101015); 0.25% collagenase IV (Worthington, Cat#LS004188) and 7.5 µg/mL DNase I (Sigma-Aldrich, Cat #D4527-10KU). Samples were incubated in a 37°C water bath for 25 min, shaking the suspension every 5-10 min. At the end of the incubation time, the sample was further dissociated using the gentle MACS dissociator system (program C; pre-programmed by manufacturer). Next, the cell suspension was filtered through a 100 µm cell strainer (Sigma-Aldrich, Cat#CLS431752-50EA) and the cell strainer was rinsed with a PBS-based wash buffer (WB; containing 0.5% BSA (BSA Fraction V, Sigma-Aldrich, Cat#10735096001), 2 mM EDTA in PBS (Thermo Fisher Scientific, Cat#14190-094)). The cell suspension was centrifuged at 300 g for 5 min. The obtained supernatant was carefully removed, transferred to a fresh Falcon tube and the pellet was resuspended in WB and filtered through a 40 µm cell strainer (Sigma-Aldrich, Cat#CLS431750-50EA). Both fractions were centrifuged again at 300 g for 5 min. The pellets were resuspended in WB, pooled and the cell suspension was filtered again through the 40 µm cell strainer. The washing steps were repeated once more. Next, the cell suspension was enriched for ECs using CD31 MicroBeads (Miltenyi Biotec, Cat#130-097-418) according to the manufacturer's instructions. CD31 enriched single cell suspension was washed with WB and stained with CD45-PE-Cy7 (clone 30-F11 Thermo Fisher Scientific, Cat#25-0451-82); CD31-FITC (clone 390; Thermo Fisher Scientific, Cat#11-0311-85) and Viable dye eFluor 450 (Thermo Fisher Scientific, Cat#65-0863-18). Doublets were gated out prior to FACS sorting. Viable, CD45<sup>-</sup>, CD31<sup>+</sup> ECs were sorted into collecting medium (10% FBS, Thermo Fisher Scientific, Cat#A38401).

#### **Spleen ECs**

After perfusion, the spleen was surgically removed, rinsed with ice-cold PBS and mashed into small pieces using a plunger of a 10 mL syringe. All pieces from one animal were transferred into a 50 mL Falcon tube containing digestion medium (KnockOut™ DMEM (Thermo Fisher Scientific, Cat#10829018); 1x penicillin/streptomycin (Thermo Fisher Scientific, Cat#15140122); 2x Antibiotic-Antimycotic (Thermo Fisher Scientific, Cat#15240062); 1 mM sodium pyruvate (Thermo Fisher Scientific, Cat#1360070); 1x MEM Non-Essential Amino Acids Solution (Thermo Fisher Scientific, Cat#11140035) supplemented with 0.1% collagenase II (Thermo Fisher Scientific, Cat#17101015); 0.25% collagenase IV (Worthington, Cat#LS004188) and 7.5 µg/mL DNase I (Sigma-Aldrich, Cat #D4527-10KU). Samples were incubated at 37°C in a water bath for 15 min, shaking every 5-10 min. At the end of the incubation time a PBS-based wash buffer (WB; containing 0.5% BSA (BSA Fraction V, Sigma-Aldrich, Cat#10735096001), 2 mM EDTA in PBS (Thermo Fisher Scientific, Cat#14190-094)) was added to the digested tissue suspension and filtered first through a 100 µm cell strainer (Sigma-Aldrich, Cat#CLS431752-50EA) and then immediately re-filtered through a 40 µm cell strainer (Sigma-Aldrich, Cat#CLS431750-50EA). The cell suspension was centrifuged at 300 g for 7 min. The obtained pellet was resuspended in WB, divided into two fractions and further centrifuged using Ficoll-Paque (GE Life Sciences, Cat#17144002) gradient at 700 g for 30 min. The Ficoll fraction was then collected and diluted with WB. The cell suspension was centrifuged at 300 g for 10 min and the washing step was repeated once more. Next, the cell suspension was depleted of CD45<sup>+</sup> cells using CD45 MicroBeads (MACS Technology, Miltenyi Biotec, Cat#130-052-301) and LD columns (MACS Technology, Miltenyi Biotec, Cat #130-042-901) according to the manufacturer's instructions. Following this step, the CD45 depleted cell suspension was enriched for ECs using CD31 MicroBeads (Miltenyi Biotec, Cat#130-097-418) according to the manufacturer's instructions. The CD31 enriched single cell suspension was washed with WB and stained with CD45-PE-Cy7 (clone 30-F11 Thermo Fisher Scientific, Cat#25-0451-82); CD31-FITC (clone 390; Thermo Fisher Scientific, Cat#11-0311-85); CD11b-PE (clone M1/70, BioLegend, Cat#101208) and Viable dye eFluor 450 (Thermo Fisher Scientific, Cat#65-0863-18). Doublets were gated out prior to FACS sorting. Viable CD45<sup>-</sup> CD11b<sup>-</sup> CD31<sup>+</sup> ECs were sorted into collecting medium (10% FBS, Thermo Fisher Scientific, Cat#A38401).

#### **Testis ECs**

After perfusion, testes were surgically dissected and the epididymis was removed. Next, testes were mashed into small pieces using a plunger of a 10 mL syringe. Tissue was transferred into a 50 mL Falcon tube containing digestion medium (KnockOut™ DMEM (Thermo Fisher Scientific, Cat#10829018); 1x penicillin/streptomycin (Thermo Fisher Scientific, Cat# 15140122); 2x Antibiotic-Antimycotic, (Thermo Fisher Scientific, Cat#15240062); 1mM sodium pyruvate (Thermo Fisher Scientific, Cat#1360070); 1x MEM

Non-Essential Amino Acids Solution (Thermo Fisher Scientific, Cat#11140035) supplemented with 0.2% Collagenase Type I (Sigma-Aldrich, #C9891) and 7.5 µg/mL DNase I (Sigma-Aldrich, #D4527-10KU). Samples were incubated at 37°C in a water bath for 20 min, shaking every 5-10 min. At the end of the incubation time a PBS-based wash buffer (WB; 0.5% BSA (BSA Fraction V, Sigma-Aldrich, Cat#10735096001), 2 mM EDTA in PBS (Thermo Fisher Scientific, Cat#14190-094)) was added to the digested tissue suspension and filtered first through a 100 µm cell strainer (Sigma-Aldrich, Cat# CLS431752-50EA) and then immediately filtered through a 40 µm cell strainer (Sigma-Aldrich, Cat# CLS431750-50EA). Samples were centrifuged at 300 g for 7 min. The washing step was repeated once more. Next, the cell suspension was enriched for ECs using CD31 MicroBeads (Miltenyi Biotec, Cat#130-097-418) according to the manufacturer's instructions. The CD31 enriched single cell suspension was washed with WB and stained with CD45-PE-Cy7 (clone 30-F11 Thermo Fisher Scientific, Cat#25-0451-82); CD31-FITC (clone 390; Thermo Fisher Scientific, Cat#11-0311-85) and Viable dye eFluor 450 (Thermo Fisher Scientific, Cat#65-0863-18). Doublets were gated out prior to isolation. Viable CD45<sup>-</sup> CD31<sup>+</sup> ECs were sorted into collecting medium (10% FBS, Thermo Fisher Scientific, Cat#A38401).

#### **Small intestine ECs**

After perfusion, intestines were surgically removed, rinsed with ice-cold HBSS (Thermo Fisher Scientific, Cat#14025092) and fecal matter was flushed out with HBSS using a 20 mL syringe and an elastic protecting insert from a 18G needle (Insyte-W; 1.3x45mm). The tissue was opened longitudinally, cut into very small pieces and transferred to 50 mL Falcon tube containing pre-digestion buffer (5 mM EDTA; 5% FBS; 1.5 mM 1,4-Dithiothreitol (DTT) (Sigma-Aldrich, Cat#1019777001) in HBSS). Samples were incubated at 37°C in a water bath for 20 min, shaking every 5-10 min. Next, the pre-digested tissue was sieved through a 100 µm strainer (Sigma-Aldrich, Cat#CLS431752-50EA) and undigested small intestine was transferred to a fresh 50 mL Falcon tube containing pre-digestion buffer. The digestion step was repeated. The undigested intestine was collected, transferred again to a fresh 50 mL Falcon tube containing HBSS only and incubated at 37°C in a water bath for 20 min to ensure further digestion and removal of DTT. After this incubation step, the sample was strained through a 100 µm strainer and transferred to a gentleMACS C tube (Miltenyi Biotec, Cat#130-096-334) containing prewarmed digestion medium (KnockOut™ DMEM (Thermo Fisher Scientific, Cat#10829018); 1 x penicillin/streptomycin (Thermo Fisher Scientific, Cat#15140122); 2x Antibiotic-Antimycotic (Thermo Fisher Scientific, Cat#15240062); 1 mM sodium pyruvate (Thermo Fisher Scientific, Cat#1360070); 1x MEM Non-Essential Amino Acids Solution (Thermo Fisher Scientific, Cat#11140035) supplemented with 0.1% collagenase II (Thermo Fisher Scientific, Cat#17101015); 0.25% collagenase IV (Worthington, Cat#LS004188); 2.5 U/mL Dispase (Thermo Fisher Scientific, Cat#171055-041) and 7.5 µg/mL DNase I (Sigma-Aldrich #D4527-10KU). Intestines were further dissociated using the gentle MACS dissociator system (MACS Technology, Miltenyi Biotec) using the 37C\_m\_LPDK\_1 protocol (pre-programmed by the manufacturer). Next, the cell suspension was washed with a PBS-based wash buffer (WB; containing 0.5% BSA (BSA Fraction V, Sigma-Aldrich, Cat#10735096001), 2 mM EDTA in PBS (Thermo Fisher Scientific, Cat#14190-094)) and filtered through a 100 µm cell strainer. Samples were centrifuged for 10 min at 300 g. The washing steps were repeated until the supernatant was clear. Next, the cell suspension was enriched for ECs using CD31 MicroBeads (Miltenyi Biotec, Cat#130-097-418) according to the manufacturer's instructions. The CD31 enriched single cell suspension was washed with WB and stained with CD45-PE-Cy7 (clone 30-F11 Thermo Fisher Scientific, Cat#25-0451-82); CD31-FITC (clone 390; Thermo Fisher Scientific, Cat#11-0311-85) and Viable dye eFluor 450 (Thermo Fisher Scientific, Cat#65-0863-18). Doublets were gated out prior to FACS sorting. Viable CD45<sup>-</sup> CD31<sup>+</sup> ECs were sorted into collecting medium (10% FBS, Thermo Fisher Scientific, Cat#A38401).

#### **Liver ECs**

After perfusion, the liver was surgically dissected, rinsed in ice-cold PBS and liver lobes were separated. Tissue was transferred into a 50 mL Falcon tube containing digestion medium (KnockOut™ DMEM (Thermo Fisher Scientific, Cat#10829018); 1x penicillin/streptomycin (Thermo Fisher Scientific, Cat#15140122); 2x Antibiotic-Antimycotic (Thermo Fisher Scientific, Cat#15240062); 1mM sodium pyruvate (Thermo Fisher Scientific, Cat#1360070); 1x MEM Non-Essential Amino Acids Solution (Thermo Fisher Scientific, Cat#11140035) and supplemented with 0.1% collagenase I (Thermo Fisher Scientific, Cat#17018029) and 0.1% collagenase II (Thermo Fisher Scientific, Cat#17101015), 2.5 U/mL Dispase (Thermo Fisher Scientific, Cat#171055-041) and 7.5 µg/mL DNase I (Sigma-Aldrich #D4527-10KU). Samples were incubated at 37°C in a water bath for 30 min, shaking every 5-10 min. At the end of the incubation time a PBS-based wash buffer (WB; containing 0.5% BSA (BSA Fraction V, Sigma-Aldrich, Cat#10735096001), 2 mM EDTA in PBS (Thermo Fisher Scientific, Cat#14190-094)) was added and the cell suspension was filtered through a 100 µm cell strainer (Sigma-Aldrich, Cat#CLS431752-50EA) and centrifuged at 300 g for 7 min. The obtained pellet was resuspended in WB and filtered through a 40 µm cell strainer (Sigma-Aldrich, Cat#CLS431750-50EA). Samples were centrifuged at 300 g for 7 min. The washing step was repeated once more. Next, the cell suspension was enriched for ECs using CD31 MicroBeads (Miltenyi Biotec, Cat#130-097-418) according to the manufacturer's instructions. The CD31 enriched single cell suspension was washed with WB and stained with CD45-PE-Cy7 (clone 30-F11 Thermo Fisher Scientific, Cat#25-0451-82); CD31-FITC (clone 390; Thermo Fisher Scientific, Cat#11-0311-85); CD11b-PE (clone M1/70, BioLegend, Cat#101208) and Viable dye eFluor 450 (Thermo Fisher Scientific, Cat#65-0863-18). Doublets were gated out prior to FACS sorting. Viable, CD11b<sup>-</sup> CD31<sup>+</sup> ECs were sorted into collecting medium (10% FBS, Thermo Fisher Scientific, Cat#A38401).

#### **Muscle ECs**

After perfusion, the hindlimb skeletal muscles were surgically removed. Soleus and extensor digitorum longus (EDL) were dissected and kept separately throughout the entire procedure. Single muscles were transferred to a Petri dish chilled on ice and were minced with a scalpel until a homogeneous paste-like slurry was formed. The tissue was transferred to a Falcon tube and further digested in

digestion medium (KnockOut™ DMEM (Thermo Fisher Scientific, Cat#10829018); 1x penicillin/streptomycin (Thermo Fisher Scientific, Cat#15140122); 2x Antibiotic-Antimycotic (Thermo Fisher Scientific, Cat#15240062); 1mM sodium pyruvate (Thermo Fisher Scientific Cat#1360070); 1x MEM Non-Essential Amino Acids Solution (Thermo Fisher Scientific Cat#11140035) and supplemented with 0.2% collagenase IV (Worthington, Cat#LS004188), 1.25 U/mL Dispase (Thermo Fisher Scientific, Cat#171055-041), 7.5 µg/mL DNase I (Sigma-Aldrich, Cat#D4527-10KU) and 2 mM CaCl<sub>2</sub> in the HulaMixer rotator (12 rpm) at 37°C for 45 min. Every 15 min, muscle tissue was further mechanically homogenized by pipetting up and down for a few minutes with a glass Pasteur pipette with a narrow tip (VWR, Cat#612-3813). At the end of the incubation time a PBS-based wash buffer (WB; containing 0.5% BSA (BSA Fraction V, Sigma-Aldrich, Cat#10735096001), 2 mM EDTA in PBS (Thermo Fisher Scientific, Cat#14190-094)) was added to the cell suspension and the digested tissue was filtered first through a 70 µm cell strainer (Sigma-Aldrich, Cat#CLS431751-50EA) and then through a 40 µm cell strainer (Sigma-Aldrich, Cat#CLS431750-50EA). Samples were centrifuged at 300 g for 20 min. Next, the cell suspension was enriched for ECs using CD31 MicroBeads (Miltenyi Biotec, Cat#130-097-418) according to the manufacturer's instructions. The CD31 enriched single cell suspension was washed with WB and stained with CD45-PE-Cy7 (clone 30-F11 Thermo Fisher Scientific, Cat#25-0451-82); CD31-FITC (clone 390; Thermo Fisher Scientific, Cat#11-0311-85) and Viable dye eFluor 450 (Thermo Fisher Scientific, Cat#65-0863-18). Doublets were gated out prior to isolation. Viable CD45<sup>-</sup> CD31<sup>+</sup> ECs were sorted into collecting medium (10% FBS, Thermo Fisher Scientific, Cat#A38401).

### **Colon ECs**

After perfusion, the colon was surgically removed, rinsed with ice-cold PBS and fecal matter was flushed with 20 mL cold HBSS (Thermo Fisher Scientific, Cat#14025092) using an elastic protecting insert from a 18G needle (Insyte-W, 1.3x45mm). The colon was pinned down, opened longitudinally and using a sterile blade, the mucus was swiftly scraped out. Next, the colon was cut into very small pieces and transferred to gentleMACS C tubes (Miltenyi Biotec, Cat #130-093-237) containing digestion buffer (KnockOut™ DMEM (Thermo Fisher Scientific, Cat#10829018); 1x penicillin/streptomycin (Thermo Fisher Scientific, Cat#15140122); 2x Antibiotic-Antimycotic (Thermo Fisher Scientific, Cat#15240062); 1mM sodium pyruvate (Thermo Fisher Scientific, Cat#1360070); 1x MEM Non-Essential Amino Acids Solution (Thermo Fisher Scientific, Cat#11140035) supplemented with 0.1% collagenase II (Thermo Fisher Scientific, Cat#17101015); 0.25% collagenase IV (Worthington, Cat#LS004188), 2.5 U/mL Dispase (Thermo Fisher Scientific, Cat#171055-041) and 7.5 µg/mL DNase I (Sigma-Aldrich #D4527-10KU). Samples were incubated at 37°C in a water bath for 15 min, shaking every 5 min. At the end of the incubation time, the sample was further dissociated using the gentle MACS dissociator system (program C; pre-programmed by manufacturer) (MACS Technology, Miltenyi Biotec). The digestion reaction was stopped by addition of the same volume of PBS-based wash buffer 2 (WB2; containing 3% FBS (Thermo Fisher Scientific, Cat#A38401) and 10 mM EDTA in PBS (Thermo Fisher Scientific, Cat#14190-094)). The cell suspension was filtered through a 100 µm cell strainer (Sigma-Aldrich, Cat#CLS431752-50EA) and centrifuged at 300 g for 7 min. The washing step was repeated twice more and cells were centrifuged at 300 g for 7 min. Next, the cell suspension was enriched for ECs using CD31 MicroBeads (Miltenyi Biotec, Cat#130-097-418) according to the manufacturer's instructions. The CD31 enriched single cell suspension was washed with a PBS-based wash buffer (WB; containing 0.5% BSA (BSA Fraction V, Sigma-Aldrich, Cat#10735096001)) and stained with CD45-PE-Cy7 (clone 30-F11 Thermo Fisher Scientific, Cat#25-0451-82); CD31-FITC (clone 390; Thermo Fisher Scientific, Cat#11-0311-85) and Viable dye eFluor 450 (Thermo Fisher Scientific, Cat#65-0863-18). Doublets were gated out prior to isolation. Viable CD45<sup>-</sup> CD31<sup>+</sup> ECs were sorted into collecting medium (10% FBS, Thermo Fisher Scientific, Cat#A38401).

### **Renal ECs**

After perfusion, kidneys were surgically dissected and the capsule was removed using forceps. The tissue was placed on a Petri dish containing ice-cold HBSS (Thermo Fisher Scientific, Cat#14025092) and using a scalpel, the kidneys were cut into small pieces. The tissue was transferred to a 50 mL Falcon tube containing HBSS-based digestion buffer (HBSS (Thermo Fisher Scientific, Cat#14025092) supplemented with 0.2% Collagenase Type I (Sigma-Aldrich, Cat#C9891) and 15 µg/mL DNase I (Sigma-Aldrich #D4527-10KU). Samples were incubated at 37°C in a water bath for 40 min, shaking every 10 min. At the end of the incubation time, ice-cold HBSS buffer was added and the digested tissue suspension was filtered through a 70 µm cell strainer (Sigma-Aldrich, Cat#CLS431751-50EA). The flow-through was immediately filtered again through a 40 µm cell strainer (Sigma-Aldrich, Cat#CLS431750-50EA). The cell strainers were washed extensively with HBSS to allow tubules to be washed through the strainer mesh. The flow-through was centrifuged at 300 g for 7 min. The cell suspension was enriched for ECs using CD31 MicroBeads (Miltenyi Biotec, Cat#130-097-418) according to the manufacturer's instructions. The CD31 enriched single cell suspension was washed with wash buffer (WB; containing 0.5% BSA (BSA Fraction V, Sigma-Aldrich, Cat#10735096001), 2 mM EDTA in PBS (Thermo Fisher Scientific, Cat#14190-094)) and stained with CD45-PE-Cy7 (clone 30-F11 Thermo Fisher Scientific, Cat#25-0451-82); CD31-FITC (clone 390; Thermo Fisher Scientific, Cat#11-0311-85) and Viable dye eFluor 450 (Thermo Fisher Scientific, Cat#65-0863-18). Doublets were gated out prior to FACS sorting. Viable, CD45<sup>-</sup> CD31<sup>+</sup> ECs were sorted into collecting medium (10% FBS, Thermo Fisher Scientific, Cat#A38401). Of note, this protocol can be used for the isolation of cortex and medullar renal ECs (less for glomerular ECs).

### **Library Preparation and Sequencing**

Single cell suspensions of freshly isolated ECs were resuspended in PBS containing 0.04% ultra-pure BSA. scRNA-seq libraries were prepared using the Chromium Single Cell 3' Reagent Kits v2 (10x Genomics; Pleasanton, CA, USA) according to the manufacturer's

instructions. The aimed target cell recovery for each library was 5,000 (except for soleus, aimed recovery was 3,000 cells). Generated libraries were sequenced on an Illumina HiSeq4000, followed by de-multiplexing and mapping to the mouse genome (build mm10) using CellRanger (10x Genomics, version 2.1.1).

### Data Processing and *In Silico* EC Selection

Gene expression matrices were generated using the CellRanger software (10x Genomics). Sample data were aggregated using CellRanger software and raw data were processed further in R (version 3.4.4). The following quality control steps were performed: (i) genes expressed by less than 10 cells or with a row average of < 0.002 were not considered; (ii) cells that expressed fewer than 300 genes (low quality), and cells that expressed over 4,000 genes (potential doublets) were excluded from further analysis; (iii) cells in which over 10% of unique molecular identifiers (UMIs) were derived from the mitochondrial genome were removed. The data were normalized using the *NormalizeData* function as implemented in the Seurat package (Satija et al., 2015). For *in silico* EC selection, we first identified highly variable genes using the *Seurat FindVariableGenes* function (mean lower threshold = 0.0125, mean higher threshold = 8, dispersion threshold = 0.5. Data (using highly variable genes only) was then auto-scaled and summarized by principal component analysis (PCA) using the *flashPCA* package (Abraham et al., 2017), followed by visualization using t-Distributed Stochastic Neighbor Embedding (t-SNE, *Rtsne* package; top 8 principal components (PCs)) (van der Maaten and Hinton, 2008). Graph-based clustering was performed to cluster cells according to their gene expression profile using the *FindClusters* function in *Seurat* (clustering resolution = 1, k-nearest neighbors = 10). EC clusters were annotated based on the expression of known EC and non-EC marker genes, including *Pecam1* and *Cdh5* (vascular ECs), *Prox1* and *Lyve-1* (lymphatic ECs), *Col1a1* (fibroblasts), *Hba-a1*, *Hba-a2*, *Hbb-bs* (red blood cells) and *Acta2* (smooth muscle cells). Contaminating cell clusters (non-ECs) were removed, and all downstream analysis was performed on ECs only.

### Clustering of Tissues

For each tissue independently, we identified highly variable genes using the *Seurat FindVariableGenes* on the *in silico* selected ECs (mean lower threshold = 0.0125, mean higher threshold = 8, dispersion threshold = 0.5). We performed PCA on highly variable genes, followed by t-SNE or Uniform Manifold Approximation and Projection (UMAP) (*umap* package) (McInnes et al., 2018) visualization (top 8 PCs). We used an in-house developed tool to color-code t-SNE plots for all detected genes, to empirically define the clustering resolution for each tissue. Next, we applied graph-based clustering using the *FindClusters* function in *Seurat* (clustering resolution = 1, k-nearest neighbors = 10) and verified by t-SNE visualization that all expected clusters were captured. Clusters with highly similar expression patterns indicative to underlie the same EC phenotype were merged into the same cluster. We next identified top-ranking marker genes for each EC cluster, by performing pairwise differential gene expression analysis for each cluster against all other clusters independently, using the *limma* package (version 3.34.9) (Ritchie et al., 2015). The results of each differential analysis were ordered based on  $\log_2$  fold change (genes with the highest fold-change receiving the lowest rank number). We obtained a final ranked marker gene list for each cluster by calculating the rank product for all genes in all pairwise comparisons. To assess statistical significance, we used a recently developed algorithm to determine p values for each marker gene based on the rank product statistic (Heskes et al., 2014), and obtained Benjamini-Hochberg adjusted p values using the R package *qvalue* (Storey et al., 2015) (Table S2, S7). We screened the top 50 of these ranked marker gene lists for each identified cluster for coherent enrichment of known canonical marker genes of traditional EC subtypes (e.g., arteries, capillaries, veins, lymphatics), as well as genes involved in particular cellular pathways or processes (e.g., interferon signaling, fatty acid uptake), to facilitate putative annotation of the clusters according to a biologically meaningful phenotype. If a common putative signature was identified, we further screened the ranked marker genes lists to identify other potential candidate genes involved in the same process. Lowly sequenced clusters, or clusters that could not be unambiguously assigned to a biologically meaningful phenotype based on marker gene expression likely represent remaining low-quality cells or doublets and were removed. Moreover, clusters harboring a strong cell dissociation signature (see below) were removed if no other biologically meaningful phenotype could be assigned. For tissue-level transcriptomics analysis (Figure 1 and 2), the remaining 32,567 ECs were pooled and marker genes were identified for ECs per tissue of origin. Since LECs clustered separately from BECs in each tissue, we pooled all BEC clusters together (and separately from all LEC clusters) to identify marker genes in pooled BEC versus LEC clusters (Figure S1D, Table S2).

### Gene Set Analyses

We used Gene Set Variation Analysis (GSVA) using a collection of expert annotated vascular-related gene sets from the Molecular Signatures Database (MSigDB version 5.2 from <http://bioinf.wehi.edu.au/software/MSigDB/>) to identify pathways and cellular processes enriched in different tissues. GSVA was performed as implemented in the GSVA R-package (version 1.26.0; default parameters) (Hänzelmann et al., 2013), where the gene-by-cell matrix is converted into a gene-set-by-cell matrix. GSVA scores were calculated for sets with a minimum of 5 detected genes, all other parameters were default. As cells can be sensitive to dissociation-induced artifacts, we also performed GSVA to identify cells strongly expressing a recently published dissociation gene signature (van den Brink et al., 2017). Clusters in which this signature was detected were removed if no other marker genes that could biologically explain a stress response were expressed.

## Data Visualization

The R implementation of the *Plotly* software (<https://github.com/ropensci/plotly>) was used for t-SNE, UMAP, violin plot and bar graph visualization. The *Heatmaply* R package (version 0.15.2) (Galili et al., 2018) was used for heatmap visualization. All heatmaps were based on cluster-averaged gene expression to account for cell-to-cell transcriptomic stochastics, and data was autoscaled for visualization. Data matrices for each heatmap can be downloaded from the accompanying web tool (<https://www.vibcancer.be/software-tools/ec-atlas>).

## SCENIC

To carry out transcription factor network inference, data was subsampled by randomly selecting 835 cells from each tissue. Analysis was performed as described (Aibar et al., 2017) using the SCENIC R package (version 1.1.0, which corresponds to RcisTarget 1.2.0 and AUCell 1.4.1 with RcisTar-get mm9 motif databases). Activity of the regulatory networks was evaluated on the full dataset in the scoring step with AUCell (Step 3). Regulons annotated as “extended” include target genes harboring motifs that have been linked to the respective transcription factor by lower confidence annotations (Aibar et al., 2017).

## Comparison of Traditional EC Subtypes

To compare traditional (arterial, capillary, venous, lymphatic) ECs across tissues, EC subclusters from all tissues were pooled into: (i) artery ECs (large artery, artery EC clusters); (ii) capillary ECs (capillary EC clusters); (iii) vein ECs (large vein, vein EC clusters); (iv) lymphatic ECs (lymphatic EC clusters) (Figure 4B). ECs expressing marker genes of two vascular beds (capillary-arterial; capillary-venous), ECs that were only detected in particular tissues (angiogenic, interferon-activated, glomerular, proliferating and choroid plexus ECs), or tissues in which some traditional EC phenotypes were not detected (spleen) were excluded from this analysis (Table S4). To measure conservation of traditional EC phenotypes in the various tissues, we calculated the similarity of the top 50 marker genes using pairwise Jaccard similarity coefficients for all EC phenotypes against each other. The Jaccard similarity coefficient is defined as the size of the intersection divided by the size of the union of sets:

$$J(A, B) = \frac{|A \cap B|}{|A \cup B|} = \frac{|A \cap B|}{|A| + |B| - |A \cap B|}$$

where  $J$  is the Jaccard index and  $A$  and  $B$  are two sets of marker genes. To identify conserved versus tissue-specific marker genes for each pooled traditional EC phenotype, we calculated the median rank score of marker genes in each phenotype in every tissue. We used the following criteria to define conserved versus tissue-specific marker genes in the top 50 marker gene list: conserved markers had a median rank score < 35 and were expressed by  $\geq 80\%$  (for capillaries > 65%) of all tissues; tissue-specific markers had a median rank score < 20 and were expressed by < 25% of all tissues.

## Comparison of Tissue-Specialized EC Subtypes

To identify marker genes commonly upregulated in tissue-specialized phenotypes, we intersected the top 50 marker genes of each tissue-specialized phenotype (Table S2), followed by visualization of the intersections using *VennDiagram* (version 1.6.20; for proliferating EC phenotypes) (Chen and Boutros, 2011) or the *UpSetR* package (version 1.3.3; for interferon and angiogenic EC phenotypes) (Conway et al., 2017).

## Metabolic Gene Expression Analysis

We generated a set of 1,180 metabolic genes, detected in ECs, by combining the genes from all murine KEGG metabolic pathways selected from the Molecular Signatures Database (MSigDB version 5.2, downloaded from <http://bioinf.wehi.edu.au/software/MSigDB/>) and an in-house curated list of metabolic genes reported in the literature. All analyses were performed on a data matrix filtered for all detected metabolic genes only, and further analysis was performed as described for all genes (see above). A subset of highly variable metabolic genes was generated by intersecting the complete list of all highly variable genes ( $n = 1,462$ ) with the list of detected metabolic genes (size of intersection = 138 genes). Highly variable metabolic genes were used for hierarchical clustering and bootstrap analysis in Figure 6A, but for the illustration of metabolic gene signatures in particular tissue-specific EC phenotypes, we focused on the full set of detected metabolic genes, and on metabolic pathways of which most critical genes were upregulated.

## Pseudotime

Trajectory analysis was performed using SCORPIUS (Cannoodt et al., 2016). We included traditional EC phenotypes from the brain (shear-stress artery, interferon- and choroid plexus clusters were not included in the analysis), and performed the analysis using the top 20 marker genes for each cluster and the following parameters:  $k = 3$ , number of principal components = 8. For visualization, the clusters detected in pseudotime were smoothed using quantiles (0.25 and 0.75 for lower and upper quantiles, respectively). Clusters were ordered based on their lower quantile value; new cluster value ranges were defined by averaging together the upper quantile of the first cluster and the lower quantile of the second cluster. The newly defined cluster ranges were used for plotting. Regression span = 0.15 (local linear regression).

### Analysis of Publicly Available EC Data

For cluster prediction analysis, we used the publicly available processed data and metadata for various tissues present in the *Tabula Muris* datasets ([https://figshare.com/projects/Tabula\\_Muris\\_Transcriptomic\\_characterization\\_of\\_20\\_organs\\_and\\_tissues\\_from\\_Mus\\_musculus\\_at\\_single\\_cell\\_resolution/27733](https://figshare.com/projects/Tabula_Muris_Transcriptomic_characterization_of_20_organs_and_tissues_from_Mus_musculus_at_single_cell_resolution/27733)) (Tabula Muris Consortium et al., 2018), to avoid any discrepancies between processing and annotation of the data. In case ECs were present in both FACS- and droplet-based datasets, we selected the dataset with the highest number of ECs (droplet: kidney, muscle; FACS: lung, liver, brain, heart). For lung EC data from He et al. (He et al., 2018), raw data was extracted from GEO (accession number GEO: GSE99235) and further processed as described above. Pre-processed and normalized data as well as the accompanying metadata were extracted from the endothelial cell database (EndoDB) (Khan et al., 2019) for brain EC data from Vanlandewijck et al. (Vanlandewijck et al., 2018) and heart EC data from Zhao et al. (Zhao et al., 2018). To annotate ECs present in these various datasets, we used the *scmapCluster* algorithm as implemented in the *scmap* package (version 1.1.5) (Kiselev et al., 2018). We used the top 10 marker genes for each EC phenotype and a similarity threshold of 0.5, all other parameters were default. For the similarity threshold, the cosine similarity, Pearson and Spearman correlations were calculated. A cell can only be assigned to a phenotype when at least 2 out of these 3 calculations are > 0.5; cells that do not meet this criterion are termed ‘unassigned’. The projection was visualized using a Sankey plot, similarity scores for each phenotype were visualized using a boxplot (generated using Graphpad Prism (version 8.1.1)). To assess the expression of all conserved and tissue-specific marker genes identified in Figure 4D, we used the *Tabula Muris* datasets as described above. We generated marker gene sets harboring all conserved and tissue-specific marker genes identified for each individual tissue, and expression of marker genes enriched in ECs with a log<sub>2</sub>fold change > 0.5 are highlighted in Figure S6.

### Immunohistochemistry

Formalin-fixed paraffin-embedded murine tissue sections were subjected to immunohistochemistry. Briefly, after incubation overnight at room temperature with the primary antibodies, sections were incubated with the appropriate secondary antibodies followed by amplification with the proper tyramide signal amplification system (Perkin Elmer). For a full list of primary and secondary antibodies, see Key Resources Table. The AQP7 antibody was described previously (Nejsum et al., 2000). Nuclei were counterstained with Hoechst 33342 (Sigma-Aldrich) and slides were mounted using Prolong Gold Antifade Mountant (Thermo Fisher Scientific). Imaging was performed using a Zeiss AxioScan Z1 at 20x magnification, or by confocal imaging using a Zeiss LSM 780 confocal microscope (Carl Zeiss) at 100x magnification (alpha Plan-Apochromat 100x/1.46 Oil DIC M27). The images were processed using Fiji software (<https://fiji.sc>).

### QUANTIFICATION AND STATISTICAL ANALYSIS

To assess statistical significance for the top 50 marker genes for all tissues and EC phenotypes (Table S2), as well as for the metabolic marker genes for each tissue (Table S7), we used a recently developed algorithm to determine p values for each marker gene based on the rank product statistic (Heskes et al., 2014), and obtained Benjamini-Hochberg adjusted p values using the R package *qvalue* (Storey et al., 2015). For hierarchical clustering and bootstrap analysis, we first compiled the highly variable (metabolic) genes (2B and 6A) or top 10 marker genes of each cluster (Figure 7B) into a marker list. We calculated the mean of these marker genes and applied hierarchical clustering with Euclidean distance and complete linkage. The confidence of each branch of the tree was estimated by the bootstrap resampling approach from the R-package *pvclust* (Suzuki and Shimodaira, 2006), using a confidence score of > 0.4.

### DATA AND CODE AVAILABILITY

**DATA RESOURCES:** All raw sequencing data generated during this study are available at ArrayExpress. The accession number for the data reported in this paper is ArrayExpress: E-MTAB-8077. The published article includes all data generated or analyzed during this study. To ensure accessibility, reproducibility and resource value of the EC Atlas, we made our data available for further exploration via an interactive webtool at <https://www.vibcancer.be/software-tools/ec-atlas>. This study did not generate any unique code.

**SOFTWARE:** All software is freely or commercially available and is listed in the **STAR Methods** description and **Key Resources Table**.

# Supplemental Figures

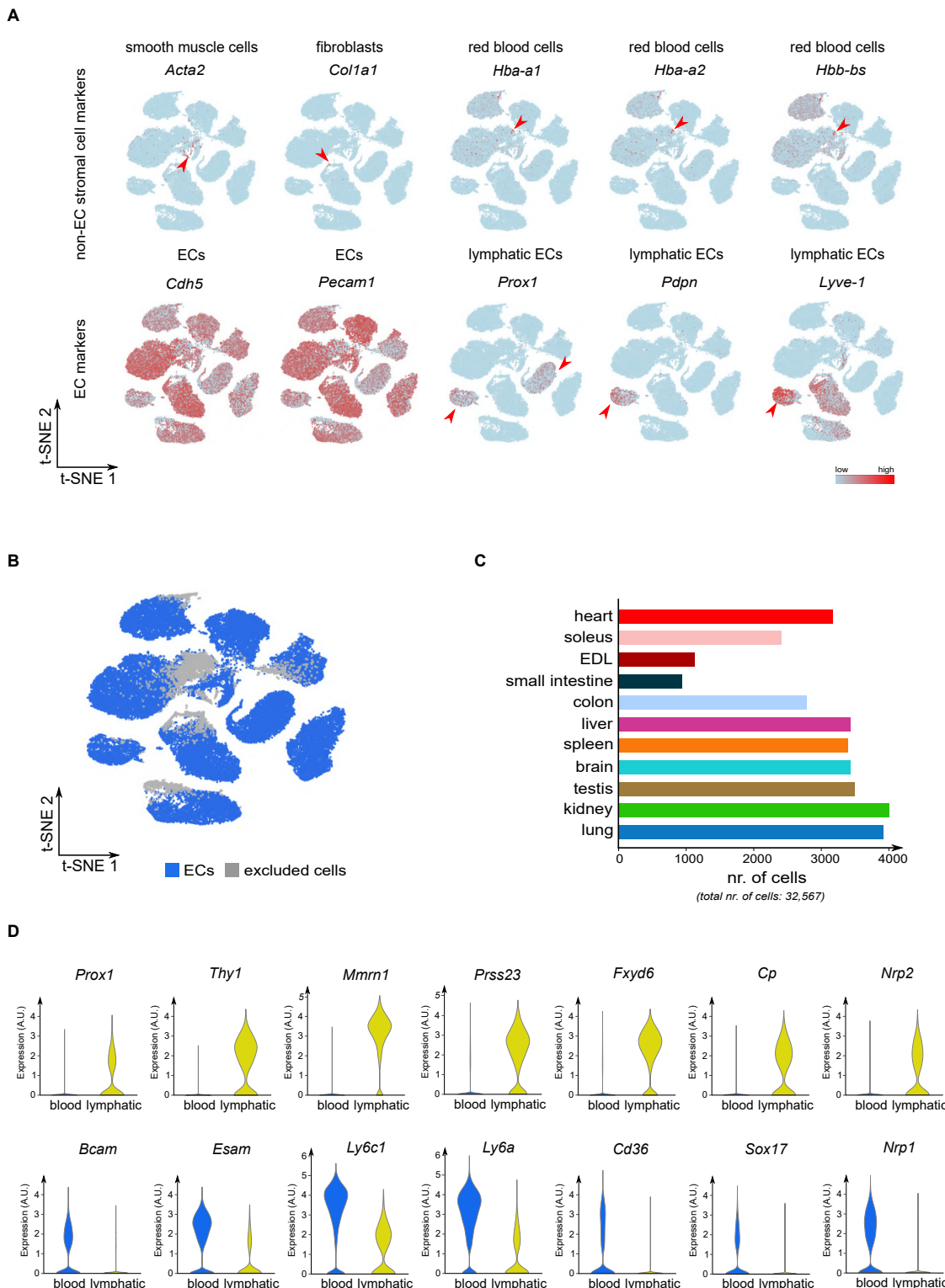


**Figure S1. In Silico EC Selection, Related to Figure 1**

(A) t-SNE plots showing pre-cleaned data; cells are color-coded for marker genes selective for smooth muscle cells (*Acta2*), fibroblasts (*Col1a1*), red blood cells (*Hba-a1*, *Hba-a2*, *Hbb-bs*), ECs (*Cdh5*, *Pecam1*) and lymphatic ECs (*Prox1*, *Pdpn*, *Lyve-1*). Arrowheads indicate cells with high expression of the indicated marker

(legend continued on next page)

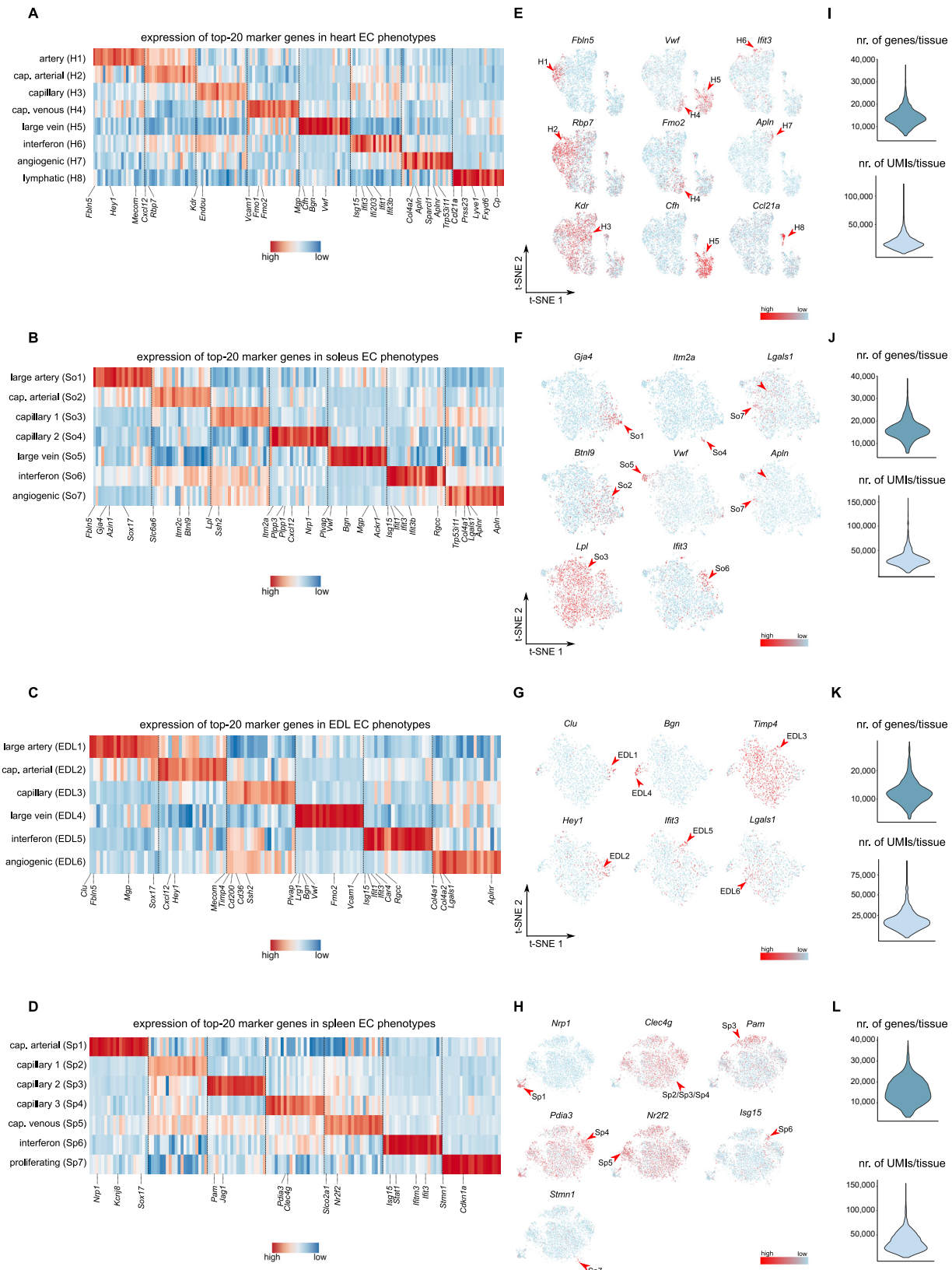
---

gene. Color scale: red, high expression; blue, low expression. Of note, marker genes for other possible contaminating populations, including leukocytes (*Ptprc*) and pericytes (*Pdgfrb*), were not detected in our dataset.

(B) t-SNE plot of cells that were included and excluded from the analysis based on expression of marker genes for ECs and other cell types. Cells of low quality (assessed by low number of genes and UMIs) were also excluded at this step. Blue indicates ECs, gray indicates excluded cells.

(C) Bar graphs showing the number of analyzed ECs per tissue isolated.

(D) Violin plots showing the expression of blood vascular EC (BEC) and lymphatic EC (LEC) specific marker genes. A.U., arbitrary units. See also Table S2.



(legend on next page)

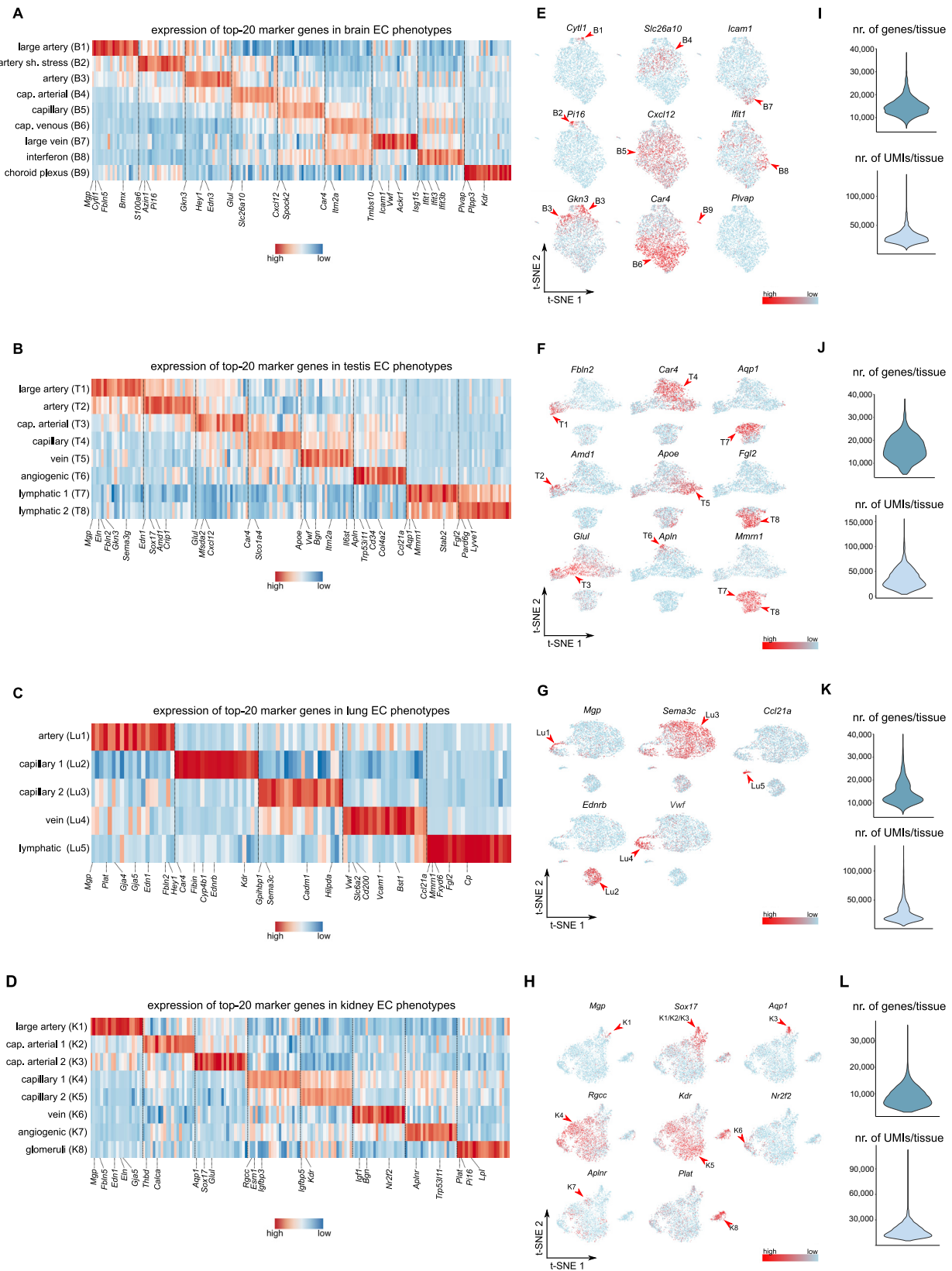
---

**Figure S2. Characterization of EC Phenotypes in Heart, Soleus, EDL, and Spleen, Related to Figure 3**

(A-D) Heatmap showing the expression of the top 20 marker genes in ECs from each cluster (identified in [Figure 3](#)) for the indicated tissue (A: heart; B: soleus; C: EDL; D: spleen). Color scale: red, high expression; blue, low expression.

(E-H) t-SNE plot, showing the expression of representative markers (shown in panels A-D) in the different clusters per tissue (identified in [Figure 3](#)). Color-coding indicates expression of the indicated marker genes for each phenotype. Color scale: red, high expression; blue, low expression.

(I-L) Violin plots, showing the distribution of genes and UMIs in each tissue. See also [Table S2](#).



(legend on next page)

**Figure S3. Characterization of EC Phenotypes in Brain, Testis, Lung, and Kidney, Related to Figure 3**

(A-D) Heatmap showing the expression of the top 20 marker genes in ECs from each cluster (identified in [Figure 3](#)) for the indicated tissue (A: brain; B: testis; C: lung; D: kidney). Color scale: red, high expression; blue, low expression.

(E-H) t-SNE plot, showing expression of representative markers (shown in panels A-D) in the different clusters per tissue (identified in [Figure 3](#)). Color-coding indicates expression of representative marker genes for each phenotype. Color scale: red, high expression; blue, low expression.

(I-L) Violin plots, showing the distribution of genes and UMIs in each tissue. See also [Table S2](#).

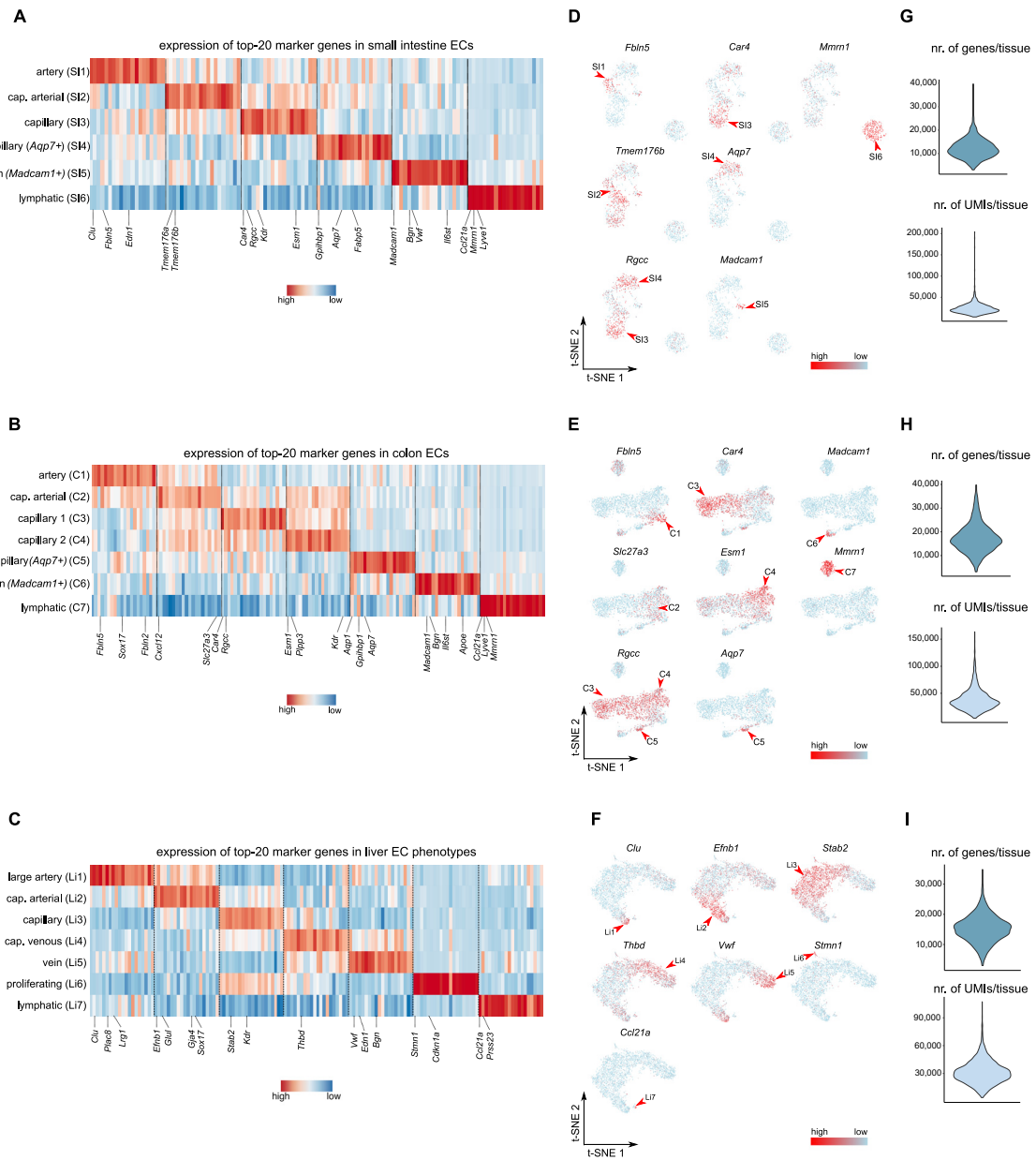
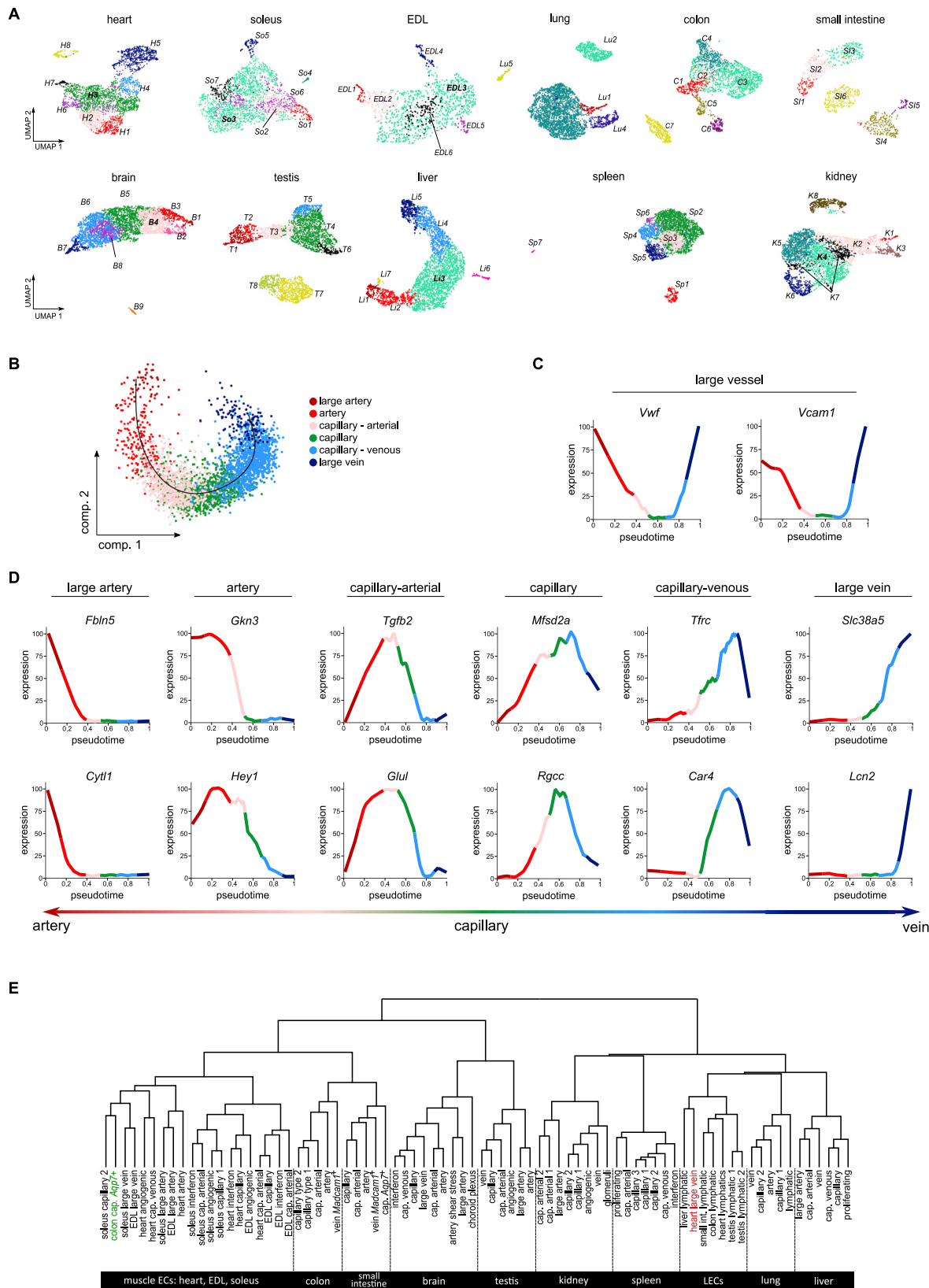


**Figure S4. Characterization of EC Phenotypes in Colon, Small Intestine, and Liver, Related to Figure 3**

(A-C) Heatmap showing the expression of the top 20 marker genes in ECs from each cluster (identified in Figure 3) for the indicated tissue (A: small intestine; B: colon; C: liver). Color scale: red, high expression; blue, low expression.

(D-F) t-SNE plot, showing expression of representative markers (shown in panels A-C) in the different clusters per tissue (identified in Figure 3). Color-coding indicates expression of representative marker genes for each phenotype. Color scale: red, high expression; blue, low expression.

(G-I) Violin plots, showing the distribution of genes and UMs in each tissue. See also Table S2.



(legend on next page)

---

**Figure S5. Vascular Bed Heterogeneity across Tissues, Related to Figures 3 and 4**

(A) UMAP visualization of tissue-specific *in silico* selected ECs. Cells are color-coded for the 78 identified EC subclusters characterized by distinct gene expression signatures. Each subcluster was numbered and labeled with the first letter(s) of the tissue name (f.i. H1 for cluster 1 in the heart UMAP). Annotations of the top-ranking marker genes of each cluster are provided in [Figures S2–S4](#).

(B) Pseudotime trajectory of the indicated brain EC phenotypes.

(C,D) Loess regression-smoothed gene expression of the indicated large vessel marker genes at opposite ends of the pseudotime trajectory (C) and gene expression of the indicated marker genes enriched in the different EC phenotypes along the artery-capillary-vein axis in pseudotime (D). Regression span = 0.15 (local linear regression). For visualization purposes, the clusters detected in pseudotime were smoothed using quantiles (0.25 and 0.75 for lower and upper quantiles, respectively). Clusters are ordered based on their lower quantile value; new cluster value ranges are defined by averaging together the upper quantile of the first cluster and the lower quantile of the second cluster. The newly defined cluster ranges are used for plotting.

(E) Dendrogram visualizing hierarchical clustering analysis of all EC subclusters from all tissues. Colors (red = heart large vein; green = colon capillary *Aqp7*<sup>+</sup>) indicate EC subclusters that did not group together with the other subclusters of their respective tissues of origin. See also [Figures S2–S4](#) and [Table S2](#).

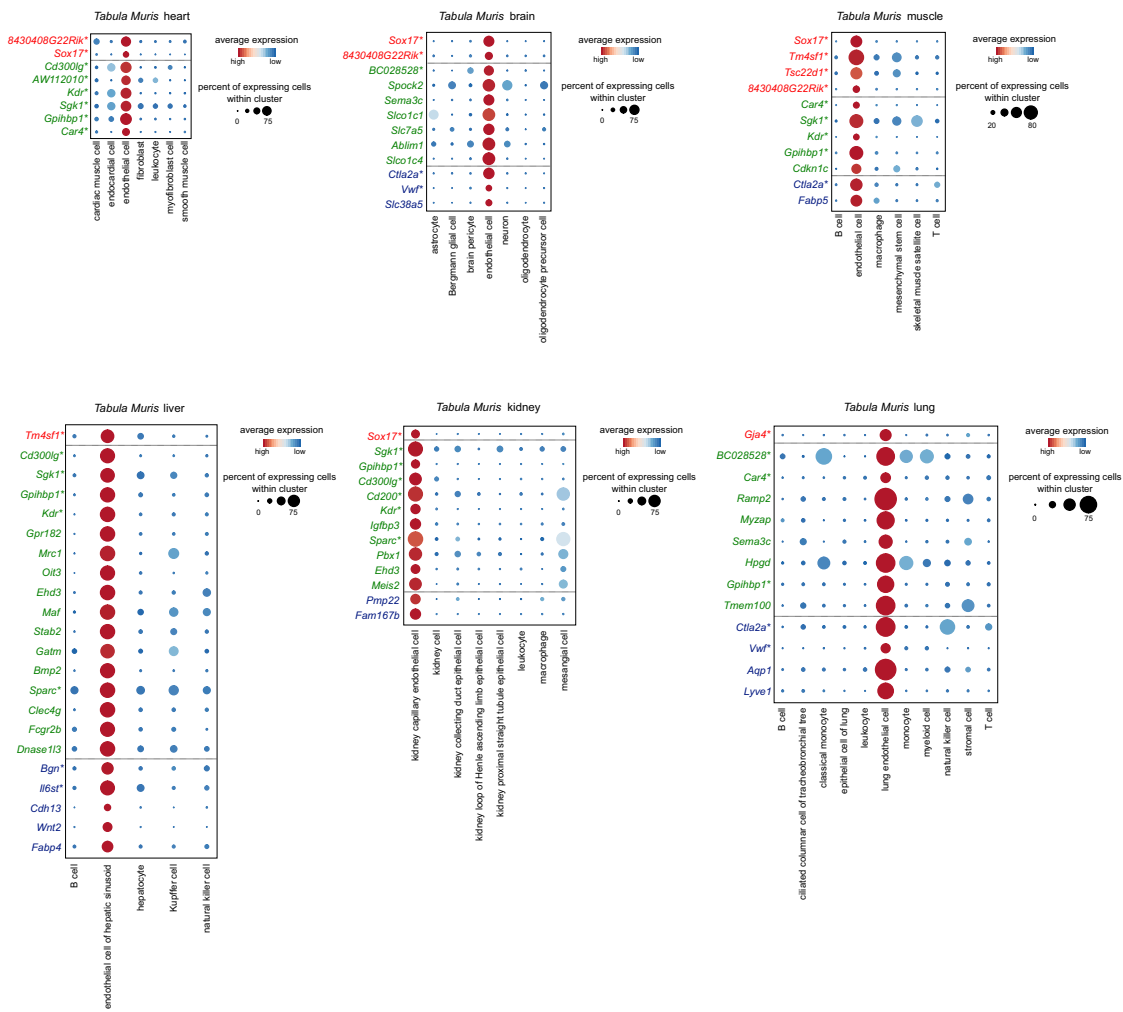


**Figure S6. Expression of EC Subcluster Marker Genes in Non-ECs, Related to Figure 4**

Dot-plot heatmaps showing the expression of conserved (asterisk) and tissue-specific EC phenotype marker genes in the *Tabula Muris* scRNA-seq datasets, from tissues containing ECs that overlap with the tissues analyzed in the EC Atlas (upper panels: heart, brain, limb muscle; lower panels: liver, kidney, lung). Only genes enriched in ECs at a log<sub>2</sub>fold change > 0.5 as compared to all other cell types are shown. Traditional EC markers are shown in color: arterial (red), capillary (green), venous (blue). The size and color intensity of each dot represent respectively the percentage of cells within each EC subcluster expressing the marker gene and the average level of expression of this marker in this EC subcluster. Color scale: red, high expression; blue, low expression. See also Table S5.

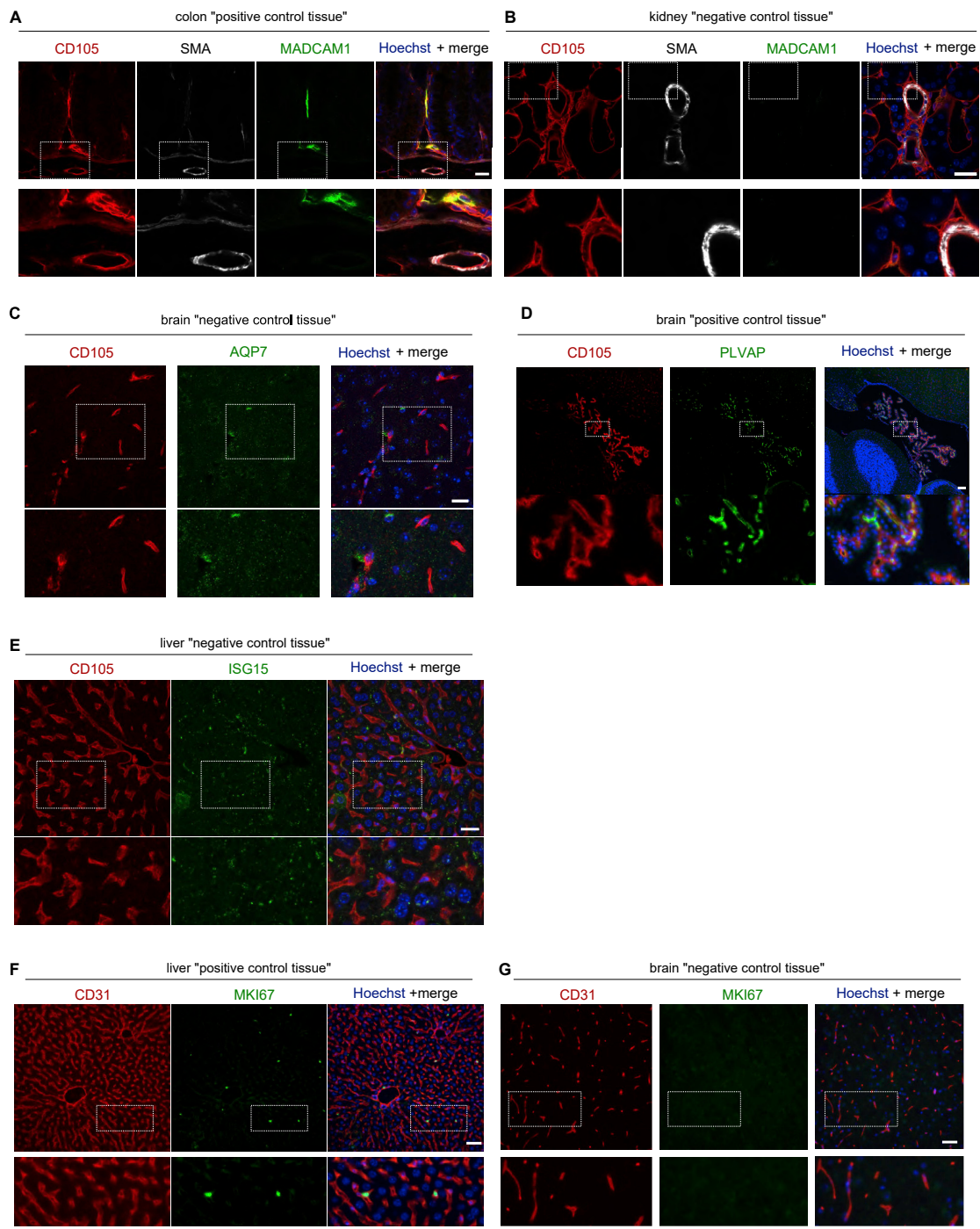


**Figure S7. Protein Validation of Specialized EC Phenotypes, Related to Figure 5**

(A,B) Representative micrographs of mouse colon (A: “positive control tissue” where *Madcam1* transcripts were detected by scRNA-seq) and kidney (B: “negative control tissue” where *Madcam1* transcripts were not detectable by scRNA-seq), immunostained for CD105 (red), MADCAM1 (green) and smooth muscle actin (SMA; gray). In colon ECs, MADCAM is detectable in thin-walled SMA<sup>-</sup> (presumably) veins/venules, but undetectable in kidney vessels.

(C) Representative micrographs of mouse brain sections (negative control tissue), immunostained for CD105 (red) and AQP7 (green).

(D) Representative micrographs of mouse brain sections (positive control tissue), immunostained for CD105 (red) and PLVAP (green).

(E) Representative micrographs of mouse liver (negative control tissue), immunostained for CD105 (red) and ISG15 (green).

(F,G) Representative micrographs of mouse liver (F; positive control tissue) and brain (G; negative control tissue), immunostained for CD31 (red) and MKI67 (green). Lower panels represent magnifications of the respective boxed areas in the upper panels. Scale bar: 25 µm (A-C,E), 100 µm (D), 50 µm (F,G). Nuclei were counterstained with Hoechst (blue) in A-G. See also Figure 5.